Synthesis and characterization of $Cs_2Sn_{1-x}Cu_xCl_6$ and $Zn_{1-y}M_yO$ (M=Cu, Co) for perovskite solar cell applications

Henok Girma Tessema

Adama Science and Technology University

Thesis Submitted to the Department of Materials Science and Engineering

School of Mechanical, Chemical, and Materials Engineering

Presented in Partial Fulfillment of the Requirement for the Degree of Masters in Materials Science and Engineering

Office of Postgraduate Studies

Adama, Ethiopia

February 2021 G.C

Synthesis and characterization of $Cs_2Sn_{1-x}Cu_xCl_6$ and $Zn_{1-y}M_yO$ (M=Cu, Co) for perovskite solar cell applications

Henok Girma Tessema

Advisor: Temesgen Debelo Desissa (Ph.D.)

Co-Advisor: Dinsefa Mensur Andoshe (Ph.D.)

Adama Science and Technology University

Department of Materials Science and Engineering

School of Mechanical, Chemical, and Materials Engineering

Presented in Partial Fulfillment of the Requirement for the Degree of Masters in Materials Science and Engineering

Office of Postgraduate Studies

Adama, Ethiopia

February 2021 G.C

Advisors Approval Sheet

To: Materials Science and Engineering Department

Subject: Thesis Submission

This is to certify that the thesis entitled "Synthesis and characterization of $Cs_2Sn_{1-x}Cu_xCl_6$ and $Zn_{1-y}M_yO$ (M=Cu, Co) for perovskite solar cell applications" which is submitted in partial fulfillment of the requirements for the degree of Masters in Materials Science and Engineering, the postgraduate program of the Department of Materials Science and Engineering, and has been carried out by Mr. Henok Girma, Id. No PGR/18434/11, under our supervision. Therefore, we recommended that the student has fulfilled the requirements and hence hereby he can submit the thesis to the department.

……	……	……..
Advisor	Signature	Date
..……	……	……..
Co-advisor	Signature	Date

Declaration

Hereby, I Henok Girma declare this M.Sc. thesis is my original work and has not been presented for any degree in any other university, and all the sources of materials used for this thesis have been duly acknowledged.

…….	...…….	…….
Student Name	Signature	Date
……	……	……..
Advisor	Signature	Date
..……	……	……..
Co-advisor	Signature	Date

Approval of Board of Examiners

We, the undersigned members of the board of examiners of the final open defense by Henok Girma Tessema ID No. PGR/18434/11 have read and evaluated his thesis entitled "Synthesis and characterization of $Cs_2Sn_{1-x}Cu_xCl_6$ and $Zn_{1-y}M_yO$ (M=Cu, Co) for perovskite solar cell applications" and examined the candidate. Therefore, this is to certify that the thesis has been accepted in partial fulfillment of the degree of Masters Science in Materials Science and Engineering.

..……	……	….……..…
Advisor	Signature	Date
……..	…….	….……
Internal Examiner and chairperson	Signature	Date
……	…….	…..…….
Internal Examiner	Signature	Date
……	…..…….	……..
External Examiner	Signature	Date
…….	……...	..……
Head of Department	Signature	Date
……...	…….	……..
School Dean	Signature	Date
……	……	……..
Postgraduate Dean	Signature	Date

Acknowledgment

First of all, I would like to thank GOD and His mother for His almightiness trough out my journey. Then, I would like to express my deep sense of gratitude and respect to my advisor Dr. Temesgen Debelo Desissa, Co-advisor Dr. Dinsefa Mensur Andoshe and for their bold, consistent, and, inspiring guidance, constructive criticism, and valuable suggestions throughout this research work. Most importantly I would like to take this opportunity to give my gratitude to Dr. Neway Medhin for her guidance and support in this work.

I would like to thank all staff members of the Materials Science and Engineering Department at Adama Science and Technology University. And then, I am deeply indebted to my family, who always believed in me and gave all their support for all of the choices that I have ever made. And my special thanks go to Mr. Demeke Tesfaye, for his amazing patience, inspiring support, and facilitation, throughout all of the lab activities of this research work. Lastly, but not least, I would also like to extend my deep gratitude to all of my staff members, especially, Mr. Andualem Merga and Ms. Biruktait Ayele, for their constructive advice, encouragement, and true friendship supports throughout this research work.

Abstract

A Photovoltaic cell (PVC) is a device that can convert light energy to electricity continuously without any required heat engine. A third-generation (organic/inorganic halide) PVC with Perovskite absorption layer (PAL) becomes a favorable material because of its high efficiency. An inorganic perovskite with a Cs_2SnCl_6 structure shows better stability, which can solve the short lifetime limitation (instability) of the cell. But a wide bandgap structured (low photo-luminescence) property of this perovskite materials makes it less efficient. In this work $Cs_2Sn_{1-x}Cu_xCl_6$ (where x=0, 0.1, 0.15, 0.2 and 0.25) PAL and $Zn_{1-y}M_yO$ (where M=Co and Cu, y=0.00, 0.01, 0.02, 0.03 and 0.05) Electron Transport Layer (ETL) was synthesized, followed by characterizations. The phase purity was analyzed by X-ray diffraction (XRD), where the PAL showed a phase pure and cubic with a space group of Fm3m. Moreover, un-doped and doped ZnO ETL showed a phase pure with Wurtzite and hexagonal crystal structure. Morphology and elemental analysis of both PAL and ETL were analyzed with Scanning Electro-Microscope (SEM) and Energy Dispersion X-ray Spectroscopy (EDS). UV-vis and Photo-Luminescence spectroscopy (PL-spectroscopy) were used for the optical property characterizations of the PAL, showing a decrease in the bandgap energy from 4.19 eV of Cs_2SnCl_6 to 3.47 eV for $Cs_2Sn_{1-x}Cu_XCl_6$ (x=0.20). Moreover, analysis of the bandgap energy of the PAL by PL spectroscopy showed a decreasing value, where a new peak formed confirming the decrease in the bandgap. Furthermore, the optical bandgap energy of un-doped and doped ZnO ETL showed a decrease in bandgap from 3.24 eV of pure ZnO to 3.06 eV, and 3.19 eV for Co-doped ZnO (Co-Z2), and Cu-doped ZnO (Cu-Z2) respectively. The Current density-voltage (J–V) measurements were performed to analyze the doping effect of ZnO ETL on $Cs_2Sn_{1-x}Cu_XCl_6$ (x=0.20) PAL device, which showed a decreasing current density as the concentration of dopant increased, and a better current measurement value was obtained for Co-doped ZnO compared to that of Cu-doped ZnO ETL.

Table of Contents

List of Figures

List of Tables

Acronyms and Abbreviations

XRD……...X-ray Diffractometer

XPS……..X-ray Photoelectron Spectroscopy

SEM…….……Scanning Electron Microscopy

EDS……..……....Energy Dispersion Spectroscopy

PL Spectroscopy……..……Photoluminescence Spectroscopy

PAL……..…….Perovskite Absorption Layer

ETL……..…….Electron Transport Layer

PCE……..…….Power Conversion Efficiency

Pure ZnO……...……ZnO

Co-Z1…….……...$Zn_{0.99}Co_{0.01}O$

Co-Z2…….…….…… $Zn_{0.98}Co_{0.02}O$

Co-Z3…….……..…….$Zn_{0.97}Co_{0.03}O$

Co-Z5…..……..…….$Zn_{0.95}Co_{0.05}O$

Cu-Z1…….……..…….…….$Zn_{0.99}Cu_{0.01}O$

Cu-Z2……...……..…… $Zn_{0.98}Cu_{0.02}O$

Cu-Z3……...……..……$Zn_{0.97}Cu_{0.03}O$

Cu-Z5…..……..……$Zn_{0.95}Cu_{0.05}O$

PDn (n=1,2,3,4,5,6,7,)……A Device using $Cs_2Sn_{1-x}Cu_xCl_6$ where x=0.20 PAL

PD1…….. …ITO/ZnO/$Cs_2Sn_{0.80}Cu_{0.20}Cl_6$/Al

PD2……...ITO/$Zn_{0.99}Co_{0.01}O$/$Cs_2Sn_{0.80}Cu_{0.20}Cl_6$/Al

PD3…… ITO/$Zn_{0.98}Co_{0.02}O$/$Cs_2Sn_{0.80}Cu_{0.20}Cl_6$/Al

PD4…… ITO/$Zn_{0.97}Co_{0.03}O$/$Cs_2Sn_{0.80}Cu_{0.20}Cl_6$/Al

PD5…….. ITO/$Zn_{0.99}Cu_{0.01}O$/$Cs_2Sn_{0.80}Cu_{0.20}Cl_6$/Al

PD6…… ITO/$Zn_{0.98}Cu_{0.02}O$/$Cs_2Sn_{0.80}Cu_{0.20}Cl_6$/Al

PD7…….. ITO/$Zn_{0.97}Cu_{0.03}O$/$Cs_2Sn_{0.80}Cu_{0.20}Cl_6$/Al

1. Introduction

1.1. Background

Energy plays a vital role in the day-to-day activities of societies; allowing them to achieve better economic development, human health, and welfare. Even if energy usage dates back to the stone age, finding more sustainable and pollution-free energy is a challenge for global society. Energy is classified into two main categories based on the sources. The first is non-renewable, which comes from fossil fuel-based sources. This energy form plays a critical role in human civilization. But it has disadvantages including a high emission of greenhouse gases and running outsource. The second is renewable energy, which a less-polluting energy source. Renewable energy can be classified into many categories depending on the form of sources, which includes hydropower, geothermal energy, ocean energy, photo-voltaic, and photo-catalytic cell [1].

A Photovoltaic cell (PVC) is a device that can convert light energy to electricity continuously without any heat engine required. PVC can be applied for power sources, communication satellites, space vehicles, water pumps, remote buildings, and solar home systems [2]. PVC or solar cell energy becomes the most novel source of energy currently and for the coming near future. A large variety of selection of materials creates a large research area in the development of a PVC. So, much research has been developed for decades to develop a solar cell device with better stability and performance. These include the first generation (Si-based solar cell material) to a second-generation material (quantum dots and thin-film solar cell) up to the third generation solar cell material. One of the third-generation solar cells is using a perovskite material as an absorption layer known as a perovskite solar cell (PSC).

PSC device shows promising evolution for the last recent decades [2, 3]. But even if it shows a tremendous evolution, long-time durability, high cost-efficiency of synthesizing, and lower stability of perovskite materials make a struggle for the breakthrough to the commercial application [4-6]. For that reason, the practical works of the PSC device further achieved only around 23% power conversion efficiency (PCE), which is still unable to meet the theoretical PCE of 31.4% [7].

1.2. Components of PSC

PSC is a multi-layered device, which contains a Perovskite Absorption Layer (PAL), a Hole Transport Layer (HTL), an Electron Transport Layer (ETL), and an Electrode. Where each component has a specific property and effects on the PSC device. A PAL is a perovskite absorption material layer most commonly in ABX_3 structure. This material can either organic or inorganic materials, where A is a large cation corresponding to 12 anions (monovalent alkali or +1 charges), where B is metal bonded to six anions (divalent metals or +2 charges) and X-is an anion bonded to A and B cations. Mostly B-site Pb halide Perovskite Absorption Layer (PAL) has become the most favorable PAL, but the device intrinsic toxicity upon device performance and device fabrication has become a fundamental challenge [8].

The high toxic Pb can be replaced by Sn ion. Then PAL with Sn halide-based organic and inorganic PAL shows promising replacement for less toxic for synthesizing of a PAL, but low stability and low efficiency again become a challenge for PSC application. The high instability issue of Sn halide PSC affects the performance due to a high oxidation state of Sn^{2+} in the atmosphere. Oxidation of Sn makes it sensitive to oxygen and moisture, which makes a less stable and efficient PSC fabrication mostly in ABX_3 structure. So a more stable structure is needed to develop a reliable PSC device. Finding stable Sn halide PSC leads to the investigation and development of morphology controlled an A_2BX_6 structure perovskite material. This structure is formed from an oxidized Sn^{2+} B-site deficient trivalent ion to a more stable form of Sn ion (Sn^{4+}). One of these materials is Cs_2SnCl_6 which shows promising stability to perform like a stable PAL for PSC device. But cannot be able to use on any device because Cs_2SnCl_6 is a wide bandgap material, which shows a lower absorption [9]. A wide bandgap makes this PAL less absorbance and energy is much larger than the absorbance range of photon energy [10]. An enhancement of Cs_2SnCl_6 is undertaken by replacing Cl^- with I^- halide and doping with heavy trivalent metals to decrease the bandgap and enhance the photoluminescence property [11-13]. Further, improvement is required to use a higher stable Cs_2SnCl_6 for the PSC device for better performance. The interface layer between PAL and ETL is the main interfacial parameter for better performance of PSC devices and therefore, enhancing ETL charge transport and carrier concentration can also enhance the performance of the PSC devices, which makes one of the other major layers in PSC device [14].

As mentioned before the Electron Transport Layer (ETL) is the main component of PSC. ETL is an n-type semiconductor material that plays a critical role in separating electrons from the electron-hole pairs, for the transfer of electrons and can be collected at the electrode for the generation of electricity. TiO_2 is the most common ETL, which shows a good property at the interface between the perovskite and ETL interface. But TiO_2 has high recombination and trap state, whereas also it requires a large synthesizing temperature than ZnO. Currently, the search for appropriate ETL lies on ZnO, which has a tremendous application and electro-optical properties such as tailorable bandgap energy. According to the intrinsic point defects theory, ZnO has an oxygen vacancy and zinc interstitial, which makes it a more favorable material due to the increase in charge density of electrons in the ZnO [15] as the positively charged oxygen vacancy and zinc interstitials has to be charge compensated by electrons. Some considered the optimizing with enhancing ETL can be able to reduce the trap states and recombination rate of electrons, cost of fabrication, and higher electron mobility, which allows large transportation of electrons through the ETL to the electrode. This can be able to enhance the performance of the PSC device. So selecting a proper ETL material and enhancing its electro-optical property is one of the alternative ways of enhancing the device's performance and stability [16, 17]. The most common way of enhancing efficiency and stability achieved by adding dopants to ETL material. Recently, doping of ZnO ETL is the most significant way of synthesizing a highly high-performance PSC device. One of these dopants is Al, which acts as a donor by replacing Zn^{2+} in the lattice due to its extra valence electron [18, 19]. Other dopants like Mg can be able to minimize the recombination rate [20]. Nitrogen-doped ZnO electron transport also shows an electron concentration enhancement [21]. Doping of ZnO with metals like Aluminum [22], Urea [23], Indium [24], and Tin [25] have been implemented for better stability and performance of PSC devices.

The other important PSC component is known as the Hole Transport Layer (HTL). HTL is a P-type doped semiconductor material used for the transfer of holes created in a PAL. Organic or inorganic HTL is mostly used for the development of PSC devices. Both HTL has low stability, which affects the general configuration of the cell. So Many Scholars agree that another way of enhancing the stability of PSC is obtained by eliminating an HTL from the PSC device. This work doesn’t contain an HTL (HTL free PSC) due to that its lower stability of perovskite materials and the high-cost requirement is the drawback of PSC device [26, 27].

Again, even if many scholars tried to enhance the efficiency and stability of a PSC device, but due to the high instability (low duration lifetime) of perovskite materials, a PSC still can't be able to meet the theoretical efficiency and commercial breakthrough. The main reason for this limitation is the challenge in the instability nature of PAL (thermal and chemical instability of organic PAL), which is degraded mainly by environmental effects like moisture and temperature of a PSC device works. But mainly the less electro-optical property of inorganic PAL affects the interface of PAL and ETL for lower electron transport. Mostly have an impact on the ETL/PAL interface of the general electrons [28-30].

As mentioned before using a Cs_2SnCl_6 PAL can provide better stability of a device, due to the stable nature of these PAL stated with some scholars. But the electro-optical property of this PAL and ZnO ETL with doping metal must be performed to enhance the performance of high unstable inorganic PSC devices. Herein, first, we synthesized an un-doped Cs_2SnCl_6 PAL and Cu doped Cs_2SnCl_6 PAL as $Cs_2Sn_{1-x}Cu_xCl_6$ (where x=0.10, 0.15, 0.20, and 0.25) followed by different characterization using different characterization methods/instruments. For ETL the un-doped ZnO and Co and Cu-doped ZnO samples were synthesized as $Zn_{1-y}M_yO$ (where M=Co and Cu also x=0.01, 0.02, 0.03, and 0.05), followed by characterizations. A PSC device was developed by a one-step spin coating method, where a selected ETL ($Zn_{1-y}M_yO$ where y=0.00, 0.02, and 0.05) is deposited using a spin coating technique on a well-cleaned ITO glass followed by a selected PAL ($Cs_2Sn_{1-x}Cu_xCl_6$ where x=0.20) is deposited on ETL. Then. Finally, a masked layer of Al electrode is deposited on the surface of the ZnO using a thermal evaporation method.

1.3. Objectives

1.3.1. General objective

Synthesis and characterizations of $Cs_2Sn_{1-x}Cu_xCl_6$ and $Zn_{1-y}M_yO$ (M=Co, Cu) for perovskite solar cell applications, followed by device fabrication and performance evaluations.

1.3.2. Specific objectives

In this work, the specific objectives are to:

- synthesis of a stable Cs_2SnCl_6 PAL material doped with different percentages of Cu by sol-gel method, followed by characterizations
- synthesis $Zn_{1-y}Cu_yO$ and $Zn_{1-y}Co_yO$ ETL, followed by characterizations
- fabricate device from the ETL and the PAL materials using a one-step spin coating method
- study electrical properties and performance of the device with dark and illumination of solar cell simulation (current density-voltage (I-V)) characteristics as well as UV-spectroscopy measurements for an optical property.

1.4. Scope

PSC device is a multi-layered device with multilayered materials, using a different selection of materials, and the interface between those layers has been done by other researchers and various studies have been undergoing in different areas. This study mainly focused only on interface engineering between ZnO and doped ZnO ETL and the Cs_2SnCl_6. Besides it is a vast study, high-cost required for synthesizing HTL, which currently free HTL PSC has become more favorable.

1.5. Significance

The significance of this study is to produce a low-cost PSC device with a stable and good electro-optical property, which can be used for commercial applications. Ethiopia is a developing country with an uprising industrial revolution. Due to that, the power required to meet the demand is increased. So as a country located at the belt of the earth, which gets unused high photon energy. So we must work on how to use this form of energy.

Chapter Two

2. Literature Review

Solar cell energy becomes a better way of generating energy by reducing a global crisis and be a renewable source of energy. Currently, it becomes applicable for the usage of producing electric power by the photovoltaic effect. The photovoltaic effect is a way of converting sunlight into electrical current by a photovoltaic cell. In these cells, two different materials (n and p-type of semiconductors) come close together to generate electric energy. When a light or some kind of radiation hits these materials it will form electrical voltage across the cell [31].

Edmond Becquerel in 1839 introduced the first photovoltaic solar cell device using an electro-chemical cell. After that, the first solar cell device has been formed by Charles Fritts in 1884 with a gold-covered selenium layer [32]. A Novel price of Albert Einstein in 1921 for photovoltaic effects makes solar cell demands increase largely. Jan Czochraski in 1918 develops a way of synthesis single crystalline silicon (First generation solar cell) [33]. Amorphous Silicon, Cadmium Indium Selenide or Tin Silicon film on Indium Tin Oxide is the most known as a second-generation solar cell with using thin-film introduced to minimize a high-cost requirement to purify silicon crystal (1^{st} generation solar cell) [32, 34].

The higher efficiency for the second generation is being achieved by Green Martin *et al.* in 2018 using Gallium Arsenide (GaAs) thin-film PCE of 28.8%. But still, 2^{nd} generation solar cell devices have limitations including environmental contamination and limited material source [34]. So to solve these limitations a solid-state solar cell with perovskite structured material is synthesized by Ryu *et al.* [35] and Kim *et al.* in 2012 [36] using a Methylammonium iodide and Methylammonium chloride absorption layer.

The first halide material $CaTiO_3$ structure is discovered by Gustav Rose in 1839 [36]. After that many kinds of research have been conducted on PSC due to the large selection of material. According to Filip and Giustino, there is approximately 2000 perovskite material with different chemical composition and crystalline structures [37]. Throughout a time using various materials selection of perovskite material shows a sensational enhance of the performance of the cell as shown in Figure 1. [38]. Even this increment can't be able to meet

the target. So many authors try to enhance the organic halide perovskite cell device using different mechanisms and material selection.

In 2014 Jeon *et al*. modify the preparation of the perovskite layer by using a mixed solvent for the synthesizing of the PAL and they found a better efficiency of 16.2% [39]. Planer architecture perovskite solar is being introduced by Liu *et al*. using the deposition of perovskite materials by two sources of thermal evaporation channel with a PCE of 13.56% [40]. But even though perovskite materials show an outstanding electro-optical property there is still some materials limitation such as low durability and high degradability in commercial applications, which is still cannot be able to meet the theoretical PCE of 31.4% mainly due to its lower stability [7].

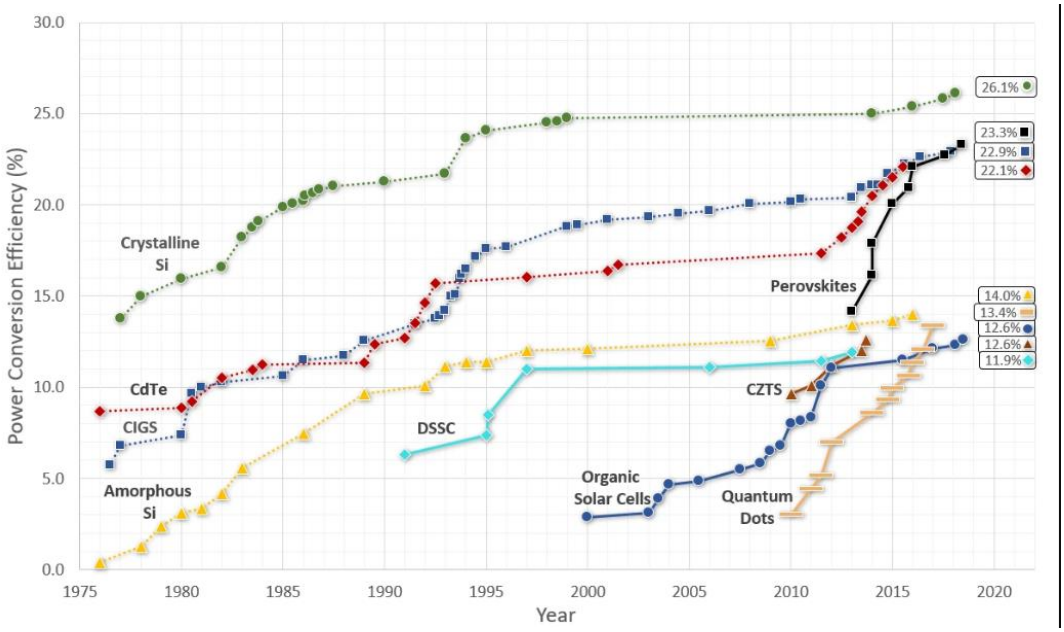

Figure 1. A Difference solar cell efficiency for the last 45 years

2.1. Working Principle

The general working principle of PSC starts with the perovskite absorption layer (PAL), where a PAL absorbs the energy known as photon energy, which then will excited (creates an electron-hole pair. These phenomena will depend on the excitation energy absorption of PAL. The energy of photons that strikes the PAL must be higher than the bandgap energy of PAL for excitation to be occurred [41].

The Electron transport layer (ETL) and Hole Transport layer (HTL) allows the transfer of electron and hole excited from the PAL. ETL allows the transfer of electrons and reducing the recombination due to the increase of electron-hole pairs [42]. The Interface and bandgap structure is the most necessary property of PSC device for better efficiency and device performance (stability) improvement. This leads to the two most favorable architectural configurations of the PSC device known as regular (*n-i-p*) and inverted (*p-i-n*) [43]. The most typical PSC consists mainly five-layer interface configuration that includes an electrode (Au or Ag), transparent conductive layer (FTO or ITO), an electron transport layer (ZnO, TiO_2, and SnO_2), a hole transport layer (spiro-oMeTAD and NiO), and perovskite layer as light absorption (Organic and Inorganic) halides [44].

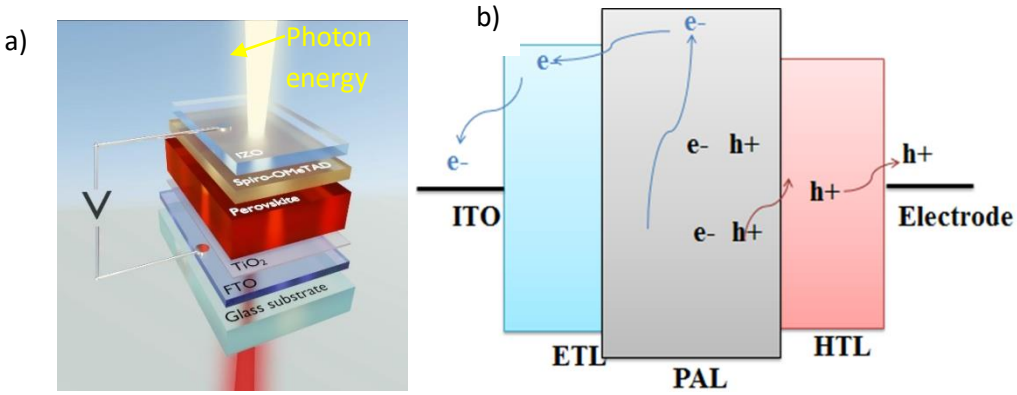

Figure 2 (a) Arrangement of the different parts of the perovskite solar cell (PSC) and (b) its corresponding energy diagram schematics

There are two basic configurations of PSC layers known as conventional and inverted configuration. Where other forms of devices, which depend on those configurations can be formed such as a mesoporous layered, ETL free, and HTL free are the common ways of device fabrication enhancing [12]. An HTL is a One way to increase the stability of the PSC device is by removing the HTL of the PSC device. Wu Qiang *et al.* developed higher efficiency with 20% PCE of using HTL free PSC. They used an inverted PSC configuration, with molecular doping of Methylammonium lead iodide PAL [45]. Meanwhile, J. Asad *et al.* grow an HTL free PSC which have a regular planar structure using Methylammonium lead iodide PAL and found efficiency of 5.7% [46].

Inverted configuration of HTL free PSC shows a remarkable development. But as Zhongmin Zhou *et al.* stated that an inverted configuration faces a problem like electron charge generation and extraction [26]. This will be the main concern for inorganic PAL device fabrication. So authors like Cuncun Wu *et al.* developed a PSC using a planar configuration

with ITO/SnO_2/$Cs_2AgBiBr_6$/P_3HT/Au configuration that showed a PCE of 1.44% [47]. Recently Dali Shao *et al.* forms a PSC device with an A_2BX_6 planar configuration of ITO/ZnO/Cs_2SnI_6/Al PSC device [48].

The basic layer in a hetero-junction PSC layer configuration used to develop a perovskite solar cell device is a perovskite absorption layer (PAL). There are two types of hetero-junction perovskite absorption layers known as an organic and inorganic perovskite absorption layer. The first organic perovskite lead halide ABX_3 PAL with two cations and anions with X site halide materials ($CH_3NH_3PbI_3$) solar device was introduced by Misaka *et al.* in a device formed by coating $CH_3NH_3PbI_3$ on a mesoporous TiO_2 electrode, which showed a PCE of 3.8% [49]. After this foundation, many research works have been published up to today. The highest PCE of 23.2% is reported by Jeon *et al.* PSC with Fluorene treatment HTL for perovskite solar cells. However, still, there is a stability issue of the device in addition to the concerns of a simple process of fabrication (Fluorene treatment) requirement for mass product and cost efficiency [50, 51]. The stability of PSC can be enhanced by enhancing the absorption layer of the device, which Seok *et al.* tried to enhance by mixing two cations perovskite layer ($FAPbI_{3(0.85)}$ and $MAPbI_{3(0.15)}$) [52]. Mixed cation halide is being so familiar for the formation of stable PSC, where Pellet *et al.* and Brivio *et al,* all can be able to form higher stable perovskite solar cell [52, 53]. Others like Tae-Hee Han *et al.* used a cross-linker (polymer-perovskite composite) to improve the stability and efficiency of PSC with a small amount of poly (propylene carbonate) (PPC) added to organic lead halide ($CH_3NH_3PbI_3$). The density functional theory (DFT) and Thermo-gravimetric analysis (TGA) result provided higher interaction energy and increased supplementation temperature [54]. Even if the organic PAL showed a better efficiency and many scholars tried to enhance the efficiency and stability, which again, organic halide PSC can't be able to break through the commercial applications. Organic halide PSC suffers a stability issue for various environmental factors like a high degradation of PSC at the interface of PAL/ETL, which is happen based on five basic factors including Moisture, intrinsic factors (defect) [55], temperature [56], UV light [57] and oxidation [58] (which all have the main factor for less stability). The uprising of the inorganic perovskite absorption layer (Inorganic PAL materials) becomes a better stable and required low-cost synthesizing materials for the device fabrication of PSC [59]. The most common type of inorganic PAL is ABX_3 structure (A= Cs^+, Se, Rb, B=Pb and Sn, X=Cl^-, I^-, Br^-). Due to its higher efficiency, Pb halide PSC is the most favorable PSC material several times. Authors like Chen *et al.* developed a high

efficient Pb halide perovskite solar cell with a PSC of 14.32%. Even if the high efficiency of using Pb at B site, this halide PSC shows that there is also a disadvantage of high toxicity due to the toxic nature of Pb. So many scholars try to replace the B-site Pb halide PSC with an Sn halide PSC [60, 61]. So Pb free $CsSnCl_3$ was first introduced by Hodes's *et al.* with a PCE of 6% [62]. The replacement of Pb with Sn shows low toxicity for PSC device fabrication [63-65]. But the higher Oxidation of Sn^{2+} makes it less stable PAL [11, 66, 67]. So a proper selection of stable Sn halide PAL material and ETL is necessary. Due to that, many researchers try to enhance the stability of $CsSnCl_3$ PAL as shown in Table 1.

Table 1 Publication on enhancing stability and electro-optical property of $CsSnCl_3$

No	Methodology	Authors	Efficiency (PCE)	Reference
1.	Systematically investigated $CsSnI_{3-x}Br_x$ Sn-based mixed halide	Sabbaet *et al.*	≈1.67%	[68]
2.	Depositing of ITO/CsSnI3/Au/Ti Schottky photovoltaic device	Chenet *et al.*	0.88%	[69]
3.	Desirable cascade energy level alignment between the inorganic perovskite and SnO2/ZnO bilayer ETL.	Yanet *et al.*	14.6%	[70]
4.	$CsPbBr_3$all-inorganic with carbon electrode and free HTL	Chenet *et al.*	-	[3]
5.	Using thermal evaporation to change γ-$CsSnI_3$ to Cs_2SnI_6	Qiu *et al.*	-	[71]
6.	A two-step Cs_2SnI_6 sequential deposition method is developed to grow high-quality	Qiu *et al.*	1%	[72]
7.	A two-step Cs_2SnCl_6 crystalline nucleated and growth from CsCl and $SnCl_2$	Zhang *et al.*	-	[9]
8.	A solution-based route synthesizing method used for Cs_2SnCl_6 nanoparticle	Scott *et al.*	-	[73]

Then A_2BX_6 perovskite structure is developed with a highly stable structure with an oxidation state of Sn^{4+}, which solves the stability problem due to oxidation at the interface [8, 11]. But this structural PAL shows a less electro-optical property and makes it a less efficient PAL [11]. Even if Lee *et al* state the electro-optical property of a perovskite material of Cs_2SnX_6 (X=I, Br, Cl) can be applied to apply for photovoltaic application. This structural perovskite material shows a high bandgap property that makes it a less usable material for PSC further application. One of these structural materials is Cs_2SnCl_6 merging as a better stable PAL with a stable form of tin 2^+ to 4^+ but the efficiency is relatively less due to the low observation coefficient (Photoluminescence property) [11].

2.2. Mechanism used to enhance the electro-optical property of Cs_2SnCl_6

2.2.1. Mixed Halide Cs_2SnCl_6

A mixed halide Cs_2SnCl_6 perovskite material of $Cs_2SnI_xCl_{6-x}$ is formed by Jie Lian *et al.* with using hydriodic acid as a different ratio between I^- and Cl^- former. This mixed halide PAL shows an enhancement in stability and PAL property whereas I^- concentration increases and the decrease of Cl^- concentration allows the decrease of the optical bandgap [74].

2.2.2. Morphology Controlled synthesizing Method

Cs_2SnCl_6 can be synthesized using a sol-gel method from CsCl and $SnCl_2$ as a Molar ratio of 2:1 respectively. This reaction will first form a $CsSnCl_3$ structure, which with further nucleation and growth (oxidation of Sn^{2+}) leads to the formation of Cs_2SnCl_6. Shuanglong Yuan *et al.* synthesized a morphology controlled Cs_2SnCl_6 by using a different amount of titrant HCl concentration. They found that as the HCl concentration increases the higher nucleation and growth will be formed. But the photoluminescence property of higher HCl concentration shows a wide emission band peak in PL spectroscopy [9].

2.2.3. Doping of B-site Deficient Sn with Metals

Another way of enhancing the electro-optical is by doping heavy trivalent metals shows a better photoluminescence property. For instance, Jinghui Li *et al.* doped Antimony (Sb) in Cs_2SnCl_6 by hydrothermal method shows an enhanced photoluminescence property [75]. Furthermore, Bi^{3+} and Mn^{2+} to deficient B–site (Sn^{4+}) developed by Zhifang tan *et al* [13] and Aifei Wang *et al* [76] respectively. The dopant of Sb^{3+} and Bi^{3+}, shows a blue shift. Whereas Mn^{2+} doping shows both blue and redshifts. So doping allows to minimizing of a wide bandgap formed on PAL to shows a blue shift (photoluminescence and electroluminescence)

property [77]. In this work we are going to synthesis Cu doped Cs_2SnCl_6 PAL to reduce a wide band gap of PAL and characterizing its electro-optical property. Also a Cu and Co doped ZnO ETL is synthesis for enhancing an electron transportation to enhanced the low efficient Cs_2SnX_6 (where X=Cl) efficiency.

2.3. Electron transport layer (ETL)

An Electron transport layer is one of the main layers of a PSC device, which can be used for splitting and transfer of electrons to the electrode to be collected for the PSC device. The electron transport layer (ETL) is the most important layer affecting the performance of the PSC device. Where TiO_2 is the most widely used ETL with an impressive PCE of 20% [14]. But recently Zinc oxide is a more favorable ETL due to it has higher electron mobility than TiO_2. ZnO is an n-type semiconductor material with unique electro-optical properties including wide bandgap, high electron mobility, strong room-temperature luminescence, good transparency, and higher energy level, which makes it the most favorable ETL material for PSC [78]. Additionally, ZnO formed with a less synthesizing process (low-temperature process), when we compared it to TiO_2 [79]. However, ZnO also has limitations of stability due to an unwanted reaction with the PSC adsorption layer. Due to this reason, formed decomposition of the absorption layer leads to unstable and reduction of efficiency of PSC device. This limitation is caused by a process of using the sol-gel process at low temperature leads to the formation of poor crystallinity leads to a trap state cause a decrease in the performance of the PSC device [80, 81].

2.3.1. Enhancing electro-optical property of ZnO ETL

Another enhancement that can be used to enhance the efficiency of a PSC device is an enhancing ETL for high electron mobility and less recombination rate. One of the most known ETL's for PSC is ZnO and TiO_2. Enhancing ZnO wide-bandgap can be used to enhance the electro-optical properties including high electron mobility, strong room-temperature luminescence, good transparency, and higher energy level. But large bandgap energy (≈3.30eV) can form narrow light absorption, the high recombination rate of the photo-generated electron-hole pairs, and charge transporting property [82]. Enhancing ZnO metal oxide ETL can be formed using different techniques, where some are described as enhancing by synthesizing method of materials, doping with impurity dopants, and device generating method using ETL, which are the common ways of enhancing their property.

2.3.1.1. Enhancing by synthesis methods

Better efficiency of PSC by enhancing the ZnO is achieved by Liang *et al.* using a Magnetron sputtering method. They find that besides ZnO, the magnetron sputtering method is a reliable way to synthesizing ETL and PSC devices [83]. But these techniques required high cost and sophisticated equipment. Other methods like the co-precipitation method are also used to enhance the property of ZnO ETL and the performance of PSC devices [84].

One of the most common ways of synthesizing metal oxide is a sol-gel method. M. Farahmandjou *et al.* used a sol-gel method to synthesis ZnO. They can be able to form a 28nm Nano-material ZnO, but still, it shows a wide bandgap of 3.49 eV [85]. A Sol-gel method is an easy way of synthesizing metal oxide (ZnO), so authors like Manasa Dogganal *et al*. uses a green synthesizing method to reduce the bandgap of ZnO. A stem extracted green synthesizing of ZnO shows a decrease in the bandgap of 3.27 eV compared to a pure ZnO of 3.45 eV [86]. But not all green synthesizing shows a decrease in the bandgap. Likewise, Haque *et al.* synthesis using *Azadirachta Indica* (Neem) showed an increase in bandgap with green synthesizing where a 3.25 eV is obtained compared to a pure ZnO of 3.23 eV bandgap [87]. So finding a reliable synthesizing method relies on doping of non-metals or metals to enhance the electro-optical property.

2.3.1.2. Enhancing by dopant method

There are two types of dopants for metal oxide semiconductors, which can enhance the electro-optical property of the semiconductor. For ZnO, both non-metal and metal types of dopants can be used for enhancing the property of performance of ZnO metal oxide ETL. Specifically One of these dopants is Al, which acts as an interstitial donor by replacing Zn^{2+} in the lattice due to its smaller size than zinc ions [18, 19]. Other dopants like Mg can be able to minimize the recombination rate [88]. Nitrogen-doped ZnO electron transport also shows an electron concentration enhancement [89]. A Fluorine and aluminum co-doped ZnO ETL film is introduced by Xinzhen *et al.*by Rf magnetron sputtering. They found that the thin film shows enhancement in crystallinity and grain size. Furthermore, the charge mobility and carrier concentration also increase [90]. But Pasquate *et al*. come with Indium doped zinc (IZO) oxide ETL on the Polymer solar cell. They used a low-temperature sol-gel process and found that with different amounts of indium doped the IZO/polymer solar cell shows only a small amount of performance enhancement. It is clearly shown that when the indium value increases the device shows no certain enhancement and also it shows a lower response for a given wavelength [91].

2.4. Synthesis Techniques

2.4.1. Physical Method

2.4.1.1. Pulsed laser deposition

In the physical Method of synthesizing ZnO ETL, it requires a high vacuum atmosphere to deposit that target material (Zinc oxide precursor) on the surface of the substrate. Pulsed laser deposition especially needs a vacuum of 10^{-8}pa and a high-power pulsed laser beam. This technique can be used to form highly flat, pure, and multi-layer films but it is an expensive technique because it requires extortionate equipment [92].

2.4.1.2. Sputtering

Sputtering also requires a high vacuum atmosphere and extortionate equipment. At ultra-high vacuum, where a highly charged ion bombarded the target material (Zinc precursor) and form a particle deposition on the surface substrate. Sputtering is also an expensive technique because it requires a high vacuum, proper sputtering power, and moderate temperature. But it is still applicable and the quickest process than pulsed laser deposition techniques [93].

2.4.2. Chemical methods

The most common of synthesizing photovoltaics cells by a chemical method is chemical vapor deposition (CVD). For metal-organic materials especially semiconductor materials, it's known as Metal-Organic Chemical Vapor Deposition (MOCVD). MOCVD can be obtained from a precursor material like zinc acetyl-acetone and reactive gases like O_2 or H_2O. The main parameter to determine the growth of ZnO thin film is the precursor material purity and the substrate. For that in this process, the substrate temperature must be between 300-500^{o}c. It means that the better perovskite of the film can be obtained at a particularly high temperature. But this is the main limitation to use MOCVD techniques, which these days a low-temperature process is necessary [94].

2.4.3. Sol-gel method

The required low-temperature process for organic-inorganic material is obtained by the sol-gel method. This method uses a solute sat dissolved into an organic solvent under a stabilizer to form a precursor solvent. Then the solution is dried and calcined at a particular temperature or the solution can be deposited on the substrate by using spin coating [93].

The thermal decomposition of inorganic salts requires a high temperature between 300-600^{0}c and organic complex zinc precursor requires a small amount of temperature. Zong *et al*. in 2018 use a two-step spin coating technique to form a planar $CH_3NH_3PbI_3$ perovskite layer. To form ZnO ETL, they use a sol-gel process technique, which is produced at low temperature but they found a relatively low PCE of 10.2% [95]. Ayi *et al* in 2018 use a sol-gel method with zinc acetate dihydric precursor at 95^{o}c. After aged and centrifuged the final product is being capped in ethanol for 30min by dispersing ZnO nanoparticles into rGO solution. The result of ZnO-NPs can be also be revealed minimizing roughness and discontinuity, which will enhance the performance but not the stability of PSC [96].

Zongtao *et al* in 2018 stated it is more preferable to modifying ZnO with suitable materials is the better alternative to modify ZnO films. So they try to enhance ZnO material by doping it with urea (CH4N2O). Using the sol-gel method urea doped zinc oxide (U-ZnO) shows a better PCE than free pure ZnO higher than 15% with a PCE of 9.5% [97]. Arafat Mahmud in 2017 doped ZnO with lithium by low-temperature sol-gel method process. The dopant shows an intercalation property in the host ZnO lattice structure that a metal unreactive interface is being formed. Due to that the PCE of the dopant layer shows a better performance than pristine ZnO ETL with a PCE of 14.07% to 16.14%. But still, it shows less transparency than pristine ZnO ETL [98].

Aluminum (Al) doped ZnO electron transporting layer is being introduced by Xingye in 2016. Then after an inverted planar Al-doped ZnO by A. Baltakesmez in 2018 and Al-doped ZnO (AZO) as TCO by Afrina in 2019 has been demonstrated. Using a low-temperature sol-gel method followed by spin coating and they all found that AZO has become the most promising material for Electron transporting layer. The surface Morphology of Aluminum doped Zinc oxide is further studied by Arun *et al* in 2018. They produced aluminum-doped zinc oxide for enhancing the ETL with a process called Ozone treatment (AZO: O_3). Ozone treatment is a process by which the aluminum-doped zinc oxide will be demonstrated under ozone gas which is allowed to reduce the oxygen vacancy. By using this method they found that aluminum-doped zinc oxide shows a better performance than an un-doped one [99].

2.4.4. One-step and two-step spin coating process

One way of easy and less cost fabrication of perovskite solar cell is a solution method known as the sol-gel method mainly followed by a one-step spin coating process. In one step spin coating process, a precursor solution is prepared by mixing halide material in polar aprotic

solvents such as N.N dimethylformamide (DMF). Then a spin coating of a precursor solution is followed by calcination at a certain temperature [100].

For controlling morphology Mitzi *et al*. in 1988 proposed a new method of fabricating perovskite solar by using a two-step spin coating method. Two-step spin coating method PbI_2/SnI_2 or $PbCl_2/SnCl_2$ first deposited on a substrate using a vacuum chamber. Then an MAI or MACl material will be deposited on it [101]. The synthesizing method can affect the property's general performance and stability. So that sol-gel methods followed by one step spin coating method is the cost-efficient way for doping of PSC and ETL for enhancing the property of the materials used.

As stated in this section, Pb free (Sn halide) PAL shows to be non-toxic PAL. But the instability of Sn^{2+} affects the general stability for device fabrication. Where Cs_2SnCl_6 PAL shows promising thermal stability for PSC device fabrication. But again this PAL shows fewer photo-luminescence and higher bandgap, which affects the photocurrent generation, electron transfer, and conductivity of the general device. Also, ZnO used as an ETL has a wide bandgap, due to that a higher recombination and lower electro-optical property is the main limitation of using ZnO. Decreasing the bandgap of both PAL and ETL can enhancing enhance the charge carrier and conductivity property of the PSC cell. So in this work, we are going to synthesis a Cu doped Cs_2SnCl_6 for reducing its bandgap and increase the photoluminescence property. Furthermore, we synthesized ZnO ETL doped with Co and Cu metals to enhance the electro-optical property of the device fabrication formed.

3. Materials and Methodology

3.1. Materials

A chemical used in this work includes Cesium chloride (CsCl) (Riedel-de Haen 99.5%), Tin powder (Carlo Erba), Zinc nitrate hexahydrate ($Zn(NO_3)_2.6H_2O$) (UNI-Chem, 98%,), Copper nitrate tri-hydrate ($Cu(NO_3)_2.3H_2O$) (Sigma Aldrich, 99%), Cobalt nitrate hexahydrate ($Co(NO_3).6H_2O$) (Labtech 97%), Sodium hydroxide (NaOH) (China 99%), Hydrochloric acid (HCl) (Pentokey 37%) and ethanol (Wase 97%) were utilized in the present work. All of the chemicals were analytical grade. Aqueous solutions were prepared using distilled water.

3.2. Experimental procedure

3.2.1. Synthesizing of Cs_2SnCl_6 and $Cs_2Sn_{1-x}Cu_xCl_6$

The undoped and doped $Cs_2Sn_{1-x}Cu_xCl_6$ (where X= 0.10, 0.15, 0.20, and 0.25) PAL was synthesized by reacting a 1:2 ratio of Tin chloride solution and Cesium chloride solution with a reactant concentration of 0.042M in H_2O and 3M of HCL. Where the dopant Cu can replace on B-site deficient, which is obtained according to the stoichiometric ratio of $Cs_2Sn_{1-x}Cu_xCl_6$ where x=0.10, 0.15, 0.20, and 0.25. All mixtures are stirred for 7 h. After that, the precipitate was collected by centrifuging the mixture, followed by washing with ethanol solvent. Finally, calcination was performed at 300 ℃ [9].

3.2.2. Synthesizing of ZnO ETL

$Zn_{1-y}M_yO$ based ETL, where (M= Cu, Co and y= 0.01, 0.02, 0.03 and 0.05) were synthesized through sol-gel method. A (1-x) Molar of Zn $(NO_3)_2.6H_2O$) and x Molar of Cu $(NO_3)_2.3H_2O$/Co $(NO_3).6H_2O$ was added to 100ml H_2O solution. Then, the mixed solution was stirred under a magnetic stirrer for 30 minutes to form the aqueous solution. After that, 2 M of NaOH was dissolved in 100 mL of distilled water, which was added to the first solution drop by drop until the pH value reached about 9 and further stirred for 2 h. Then, the gel was obtained, which was followed by centrifuging and washing with distilled water and ethanol to remove the residuals and dried in an oven at 80 ℃ for 24 h. Finally, the obtained powder was calcined at 500 ℃ and 400 ℃ for 2 h for Cu doped and Co-doped ZnO, respectively, to get the desired $Zn_{1-y}M_yO$ based catalysts [102, 103].

3.2.3. Device Fabrication Method

For the device fabrication, 1.0 M $Cs_2Sn_{1-x}Cu_xCl_6$ NPs and 0.05 M of un-doped, Co, and Cu-doped ZnO were dispersed in Dimethylformamide (DMF) solvent. A 1/3 ITO glass was etched using HCl and the ITO glass substrate was cleaned with acetone, ethanol, distilled water and dried in an ozone environment. Initially, ZnO solution was spin-coated on the top of the etched ITO glass substrate at 3000 rpm for 30 s, followed by drying at 60 °C then a second deposit at 5000 rpm for the 30s. The coated ZnO was further subjected to heating at 150 ℃ for 30 minutes. Then, the PAL solution was deposited by spin coating using 2 ramps at 1000 rpm and 2000 rpm for 10 s and 30 s, respectively. The PAL layer was subjected to heat-treatment at 220 ℃ for 4 5minutes. Then, Al electrode contact was deposited on the top of the device using a thermal evaporator [104].

3.3. Characterizations

The synthesized samples were subjected to characterizations. Determination of the crystal structure and phase purity of the samples were characterized by using an X-ray Diffraction instrument (XRD) (XRD-7000S Shimadzu). Morphology and the elemental composition were characterized by Scanning Electron Microscope (SEM) coupled with an Energy Dispersive X-ray analyzer (EDS) (COXIEM-30). The optical properties were examined by using UV-vis spectroscopy (UV-vis-3600plus Shimadzu). The thermal property was investigated by using Thermal Analysis Technique (DTG-6OH Shimadzu). A Photoluminescence property of each sample were also examined by Cary Eclipse Fluorescence Spectrophotometer Agilent Technology. Finally, for current-voltage (*I–V*) measurements, the deposited layer was cleaned for potential effective contact with an area of 0.05 cm^2 defined by the showdown mask

4. Result and Discussion

4.1. X-ray diffraction (XRD)

X-ray diffraction (XRD) analysis was undertaken to analyze the crystalline structure of the synthesized materials, where the undoped and doped PAL shows a pure and cubic crystal structure. This Cs_2SnCl_6 PAL was observed, as shown in Figure 3 of XRD patterns shows the single structure, except for the sample of $Cs_2Sn_{1-x}Cu_xCl_6$ with an *x* value of 0.25 shows secondary phases. The XRD pattern of un-doped and Cu-doped Cs_2SnCl_6 showed peaks at an angle of 14.71°, 24.11°, 28.41°, 29.75°, 34.58°, 42.62°, 45.36°, 49.64°, 52.18°, 56.01°, 59.02°, 61.89°, and 67.48° (ICSD #007-0197). The peaks of the samples doped with Cu showed a peak shift to a higher 2θ angle, which could be attributed to the replacement of Sn^{4+} (ionic radius of 2.89 Å) by Cu^{2+} (ionic radius of 0.73 Å) this causing a contraction in the lattice structure, shown in the top inset of Figure 3. This change can also be determined by analyzing the inter-planar distance and lattice parameters of each material. The inter-planar distance (*d*-spacing) showed a decreasing value according to Bragg's Law of diffraction equation, which is caused by replacing Sn^{4+} with a small ionic radius Cu, Table 2. Due to this reason, the XRD peak with different dopant concentrations shows a shift of the peaks shifting to higher 2-theta [105].

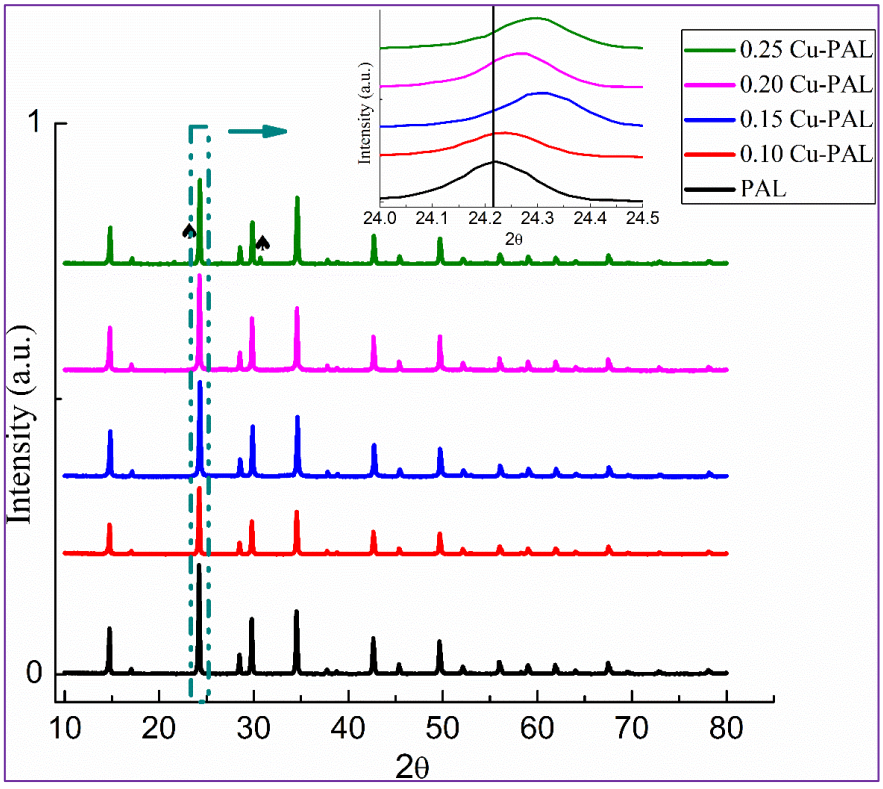

Figure 3 XRD analysis of un-doped and Cu-doped Cs_2SnCl_6 PAL

Figure 4 shows an XRD pattern for synthesized ZnO (both un-doped and doped samples), which is a phase pure (no secondary peaks for doped samples) with a hexagonal Wurtzite crystal structure. The peaks observed at a 2theta of 31.76^{o}, 34.43^{o}, 36.26^{o}, 47.57^{o}, 56.62^{o}, 62.88^{o,} and 67.96^{o} are, respectively, corresponding to a Miller index of (100), (002), (101), (102), (110), (103) and (112) crystallographic planes.

A pure Wurtzite hexagonal phase structure is formed for Co and Cu doped ZnO with a peak shift to higher 2θ for the first concentration of dopant and to lower 2θ with a further increment of the dopant concentration. The peak shift to a higher 2θ may be attributed to the compression (shrinking) as a result of ionic radii differences of the dopants, i.e., due to the replacement of Zn^{2+} (ionic radius of 0.60 Å) with Co^{2+} (ionic radius of 0.58 Å) and Cu^{2+} (ionic radius of 0.73 Å). Moreover, the peak shift could be due to the tensile stress (expanding) formed when a higher dopant concentration is distributed throughout the lattice. Furthermore, the differences in ionic radii could lead to a decrease in the inter-planar space distance (*d*-spacing) and lattice parameters as shown in Table 2. A secondary peak is also observed for $Zn_{1-y}Cu_yO$ with a Cu dopant percentage of 5%, i.e., when y=0.05, which could be the solubility limit of Cu in ZnO [105].

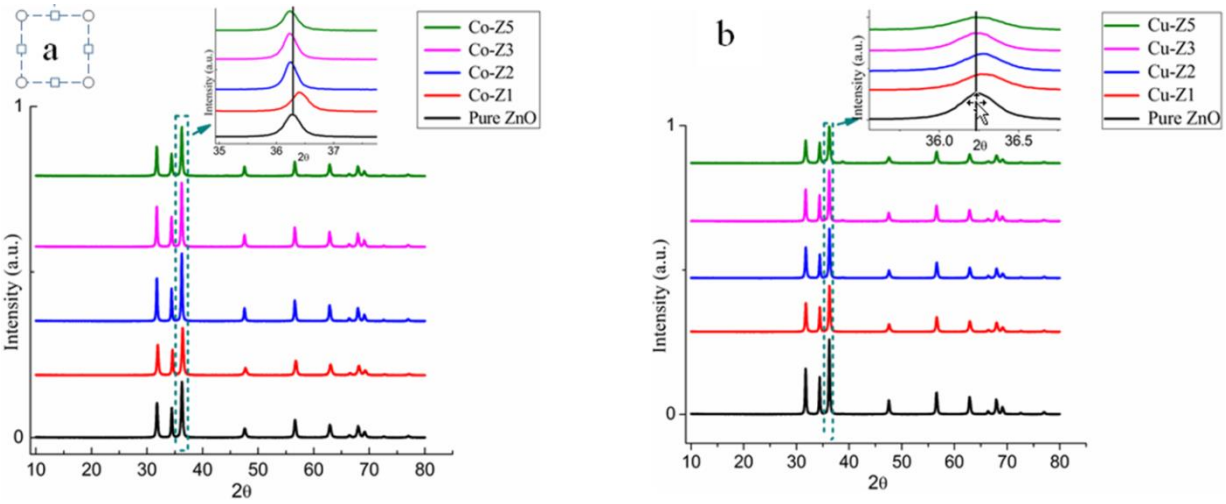

Figure 4 XRD analysis of (a) Un-doped and Co-doped ZnO, (b) undoped- Cu-ZnO

Further examination of the doping effect analyzing the *d*-spacing and lattice parameter of each of the samples with the different concentrations of dopants is undertaken which is shown in Table 2. The various *d*-spacing shown is due to the shrinkage and expansion of the lattice that will result in a peak shift in the 2θ value in XRD patterns. The *d*-spacing can be calculated using Bragg's law. For the un-doped and doped $Cs_2SnCl_{6,}$ equation (1) was used

since it is a cubic structure while equation (2) was used for ZnO ETL as it is a hexagonal structure [106, 107].

$$\frac{1}{d^2} = \frac{h^2 + k^2 + l^2}{a^2} \qquad (1)$$

$$\frac{1}{d^2} = \frac{4}{3}\left(\frac{h^2 + hk + k^2}{a^2}\right) + \frac{l^2}{c^2} \qquad (2)$$

Where (h k l) is a miller index, d is lattice constant and, a and c is a lattice constant.

The lattice parameter can also be analyzed by X-pert high score. The crystalline property of those synthesized materials in this work was analyzed and determined by using an X-pert High score as shown in Appendix 1. The difference in lattice parameter and d-spacing due to the difference in ionic radius of Sn^{2+} (ionic radius of 1.18Å) and Cu^{2+} (ionic radius of 0.73Å) for Cs_2SnCl_6 PAL. Similarly, a ZnO ETL also shows a difference in d-spacing and lattice parameters as a dopant concentration Co and Cu doped in ZnO increases. However, a small change was shown due to the similarity of ionic radius between the host and dopants Zn^{2+} (ionic radius of 0.60Å), Co^{2+} (ionic radius of 0.58Å), and Cu^{2+} (ionic radius of 0.73Å). The structural analysis indicates the effect of dopants changes the structure of the lattice, where a dopant concentration shows a slight change in the lattice distortion [108].

Table 2 d-spacing and lattice parameter values for Un-doped and doped PAL (Cs_2SnCl_6) and ETL (ZnO)

Materials	d (Å)	A	B	C
Cs_2SnCl_6	3.66662	10.3810	10.3810	10.3810
10% Cu-Cs_2SnCl_6	3.66463	10.3810	10.3810	10.3810
15% Cu-Cs_2SnCl_6	3.65407	10.3552	10.3552	10.3552
20% Cu-Cs_2SnCl_6	3.66004	10.3810	10.3810	10.3810
25% Cu- Cs_2SnCl_6	3.65623	10.3552	10.3552	10.3552
ZnO	2.47591	3.2501	3.2501	5.2071
1% Co-ZnO	2.46514	3.2417	3.2417	5.1876
2% Co-ZnO	2.47543	3.2530	3.2530	5.2130
3% Co-ZnO	2.47618	3.2530	3.2530	5.2130
5% Co-ZnO	2.47602	3.2530	3.2530	5.2130
1% Cu-ZnO	2.47356	3.2417	3.2417	5.1876
2% Cu-ZnO	2.47410	3.2501	3.2501	5.2071
3% Cu-ZnO	2.47654	3.2535	3.2535	5.2151
5% Cu-ZnO	2.47604	3.2535	3.2535	5.2121

4.2. Thermal property analysis

The thermal stability of a Cs_2SnCl_6 PAL material shows higher stability than ABX_3 PAL materials. The higher thermal stability of this PAL makes it a candidate PAL for solving short life duration for commercial applications of a PSC device. These inorganic perovskite materials show better stability based on the thermal property of the Cesium (Cs) ion [109]. The thermal analysis of a pure Cs_2SnCl_6 shows higher stability up to 627.04°c without any degradation. The thermal decomposition of un-doped and Cu-doped Cs_2SnCl_6 doesn't show a considerable change with dopant concentration. The decomposition temperature of pure Cs_2SnCl_6 formed at 627.04°C. Also, the $Cs_2Sn_{1-x}Cu_xCl_6$ measured where x=0.20 shows no significant change in thermal stability. When Cu doped at $Cs_2Sn_{1-}xCuxCl_6$ where x= 0.20 is analyzed using DTA and has a degradation temperature at 629.79°C. Additionally, there is no difference in total weight loss for both un-doped and Cu doped Cs_2SnCl_6 with 34.59% and 32.20% respectively.

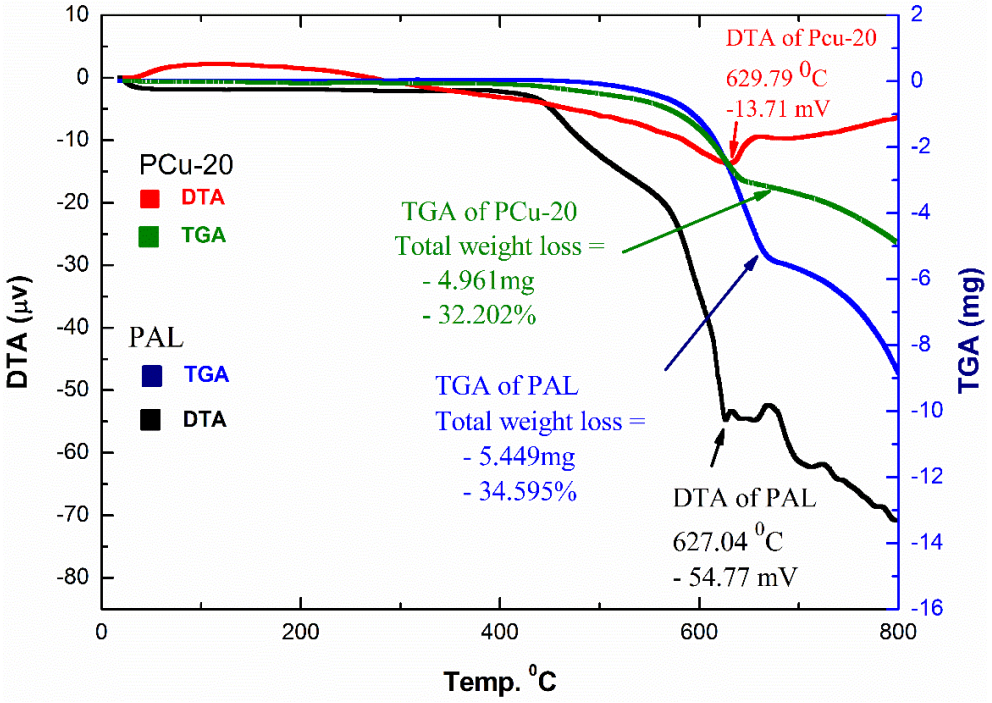

Figure 5 Thermal Analysis of Pure Cs_2SnCl_6 PAL and 0.20 Cu-Cs_2SnCl_6 PAL

The thermal analysis for ETL of ZnO shows degradation at 63.50°c due to dehydration and at 212.91°C the decomposition of nitrates from Zinc nitrate precursor to ZnO. After oxide forming the metal oxide shows a stable thermal property, which makes a favorable selection of material for ETL on thermal stability. Also, both Co and Cu doped ZnO were carried out, where the result shows degradation temperature for Co and Cu doped ZnO at 134.99°C and 137.86°C respectively due to the removal of surface water molecules (dehydration). The next

degradation temperature for 167.74℃ for Co-doped and 263.01℃ for Cu-doped ZnO, which shows the formation of oxides (ZnO) from nitrates After a formation of oxide (ZnO) the sample in both un-doped, Co and Cu doped ZnO shows a thermal stable form [110]. The TGA analysis of pure ZnO and 3% Co and Cu doped ZnO, which shows a 3% Co-doped ZnO has a less mass loss with only 2.763% relatively to Cu doped (5.421%) and pure ZnO (4.145%). This can give us the thermal stability of Co-doped ZnO shows better stability relatively.

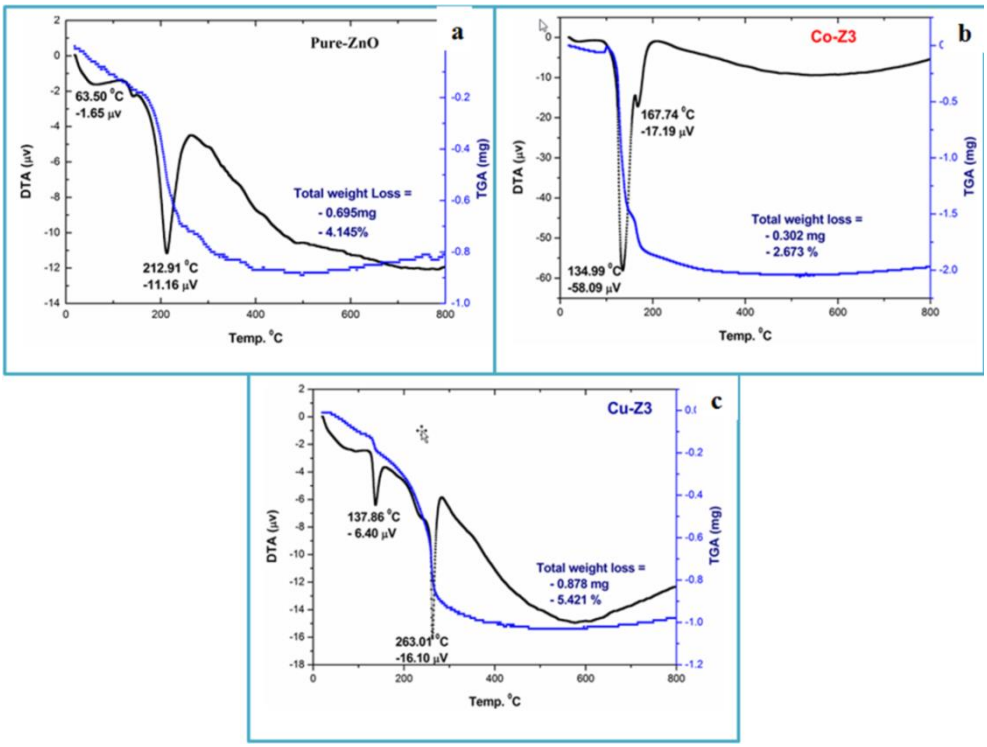

Figure 6 Thermal Analysis of (a) Pure, (b) Co and (c) Cu doped ZnO

4.3. Morphology and Elemental Analysis

Microstructural analysis of un-doped and doped of synthesized PAL and ETL sample were characterized using Scanning Electron Microscope (SEM) with a resolution of 10µm. The surface morphology of un-doped and Cu-dopedCs_2SnCl_6 shows an octahedron structure. This structure is composed of eight single-phase face-centered cubic (FCC) cubic structures. This result is consistent with morphology controlled synthesizing of Cs_2SnCl_6 by Zhang *et al.* with 3mol/L HCl concentration of a synthesizing method used for this work, which is shown in Figure 7 (a) [9]. Where Figure 7 (b) with different magnification took shows the compact growth of octahedrons structure, which fills each space with a small octahedrons phase is formed due to the crystalline growth of Cs_2SnCl_6 from $CsSnCl_3$.This tells and confirms us, as

the reaction time increases the higher nucleation growth is formed and $CsSnCl_3$ changes to Cs_2SnCl_6 structure. As shown in Figure 7 (c,d) with a different magnification comparison of a 0.20Cu-PAL, that it clearly shows a particle random distribution when a dopant of Cu is added. Which is also shows a decrease in size due to a small ionic radius of Cu (0.74Å). For elemental analysis of Cs_2SnCl_6 and 0.20Cu-PAL Energy Dispersion X-ray Spectroscopy (EDX) is used. AS shown in Figure 7 (e) a PAL (Cs_2SnCl_6) and Figure 7 (f) 0.20Cu-Cs_2SnCl_6 shows a compositional result of Cs, Sn, Cu and Cl.

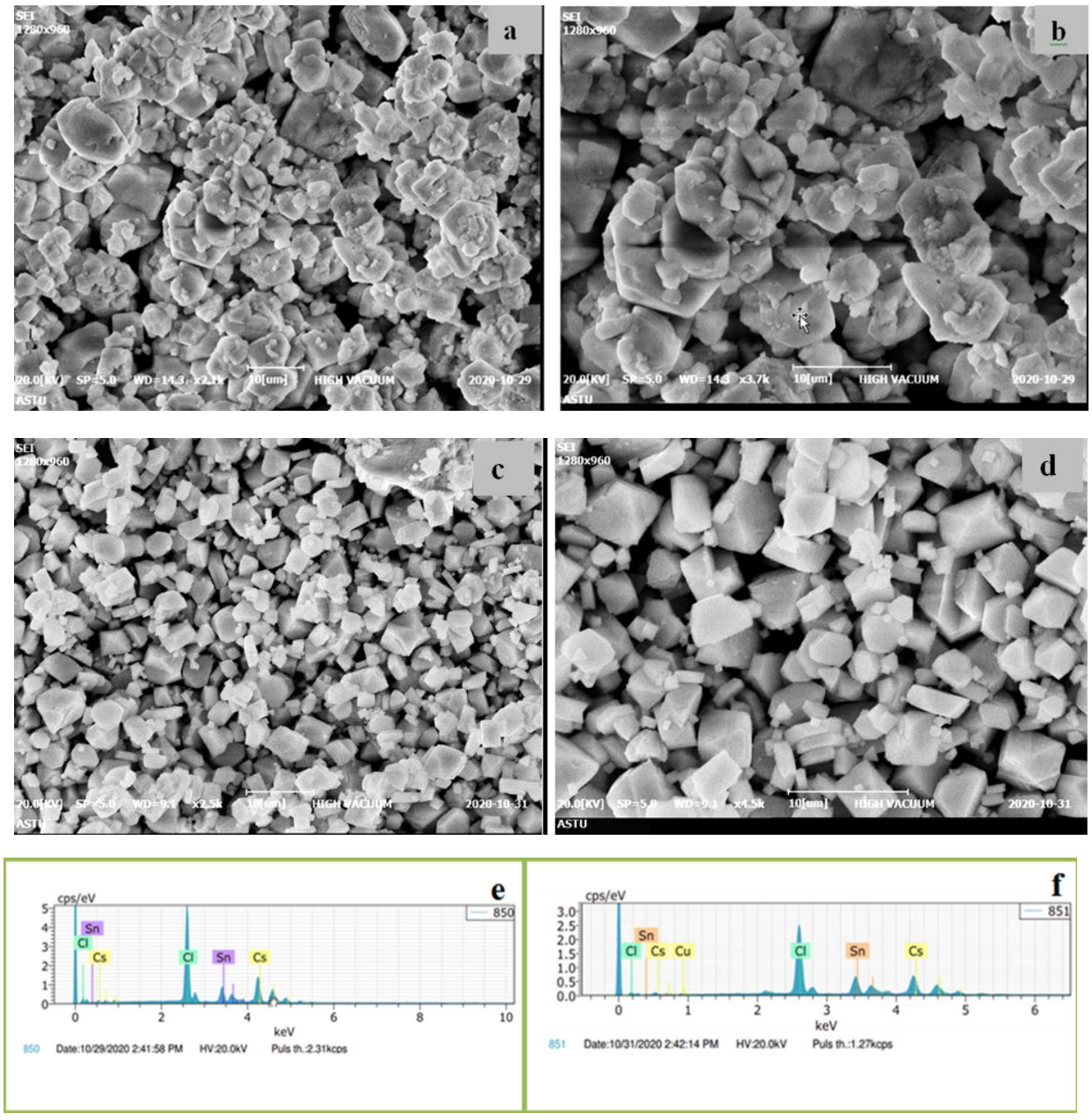

Figure 7 SEM Morphology analysis of (a,b) SEM Un-doped Pure PAL and (c,d) 0.20Cu PAL and EDX analysis of Un-doped (e) and 0.20Cu-PAL (f)

On the other hand, the morphology and elemental analysis of un-doped and doped (Co and Cu) ZnO ETL are characterized using SEM and EDX. Figure 8 (a) corresponding to the morphology of pure ZnO, where Figure 8 (b,c) shows the morphology of Co-doped ZnO (Co-Z3) and Cu-doped ZnO (Cu-Z3) respectively. The elemental analysis was also taken by EDX from the SEM analysis. The elemental analysis of a synthesized undoped and doped ZnO ETL also taken by EDX as shown in Figure 8 (d) corresponds to pure ZnO, Figure 8 (e,f), Co-doped ZnO (Co-Z3), and Cu-doped ZnO (Cu-Z3).

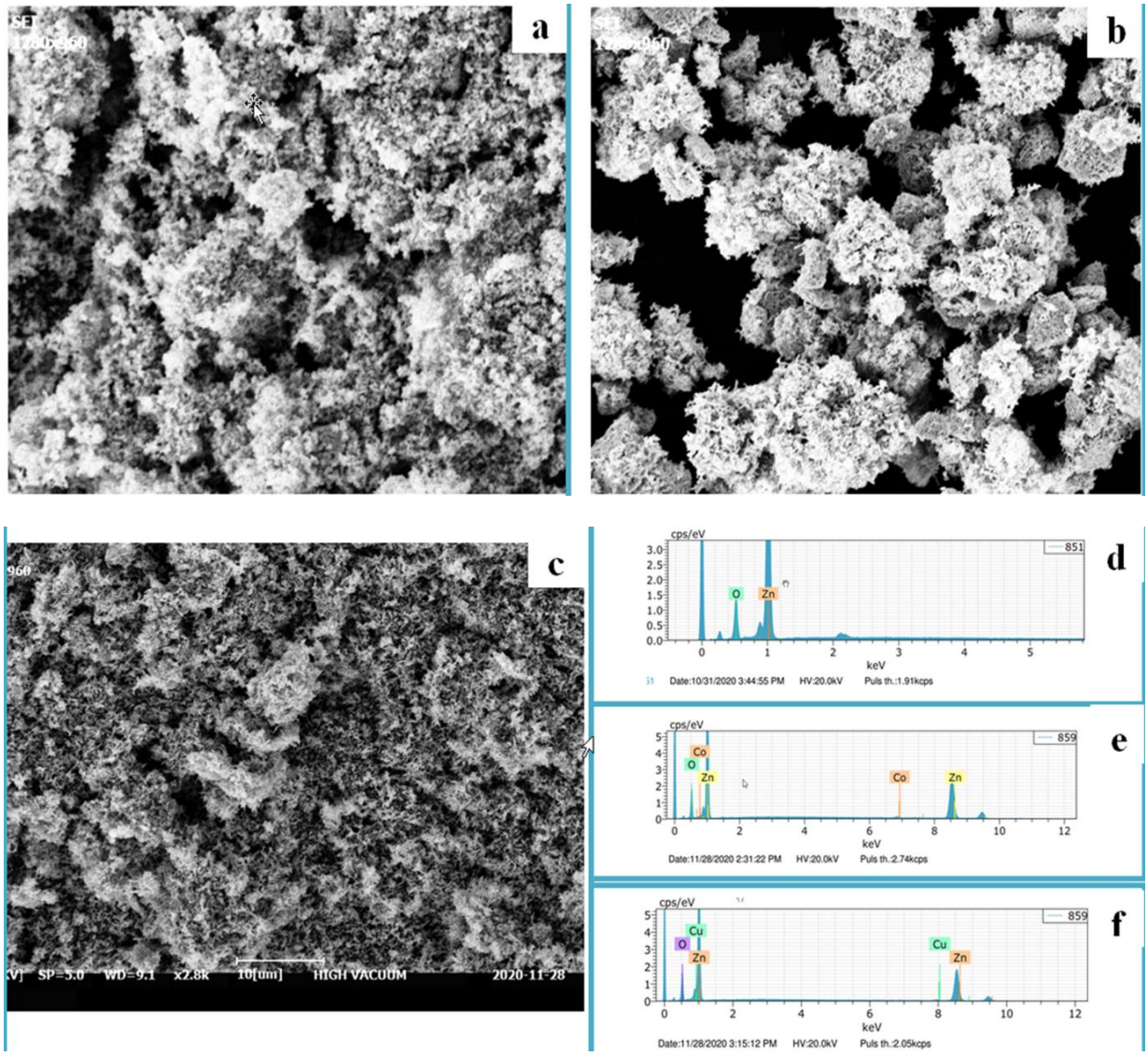

Figure 8 SEM and EDX analysis of A Pure un-doped and doped ZnO ETL (a,d) of Pure ZnO, (b,e) of Co-doped ZnO and (c,f) of Cu doped ZnO

4.4. Diffuse Reflectance Spectroscopy (DRS)

DRS analysis was be used to examine the effect of dopant concentration in the energy band structure of Un-doped and doped ZnO ETL and Cs_2SnCl_6 PAL. The bandgap of the as-synthesized materials was first analyzed with UV-Spectroscopy. Then the UV analysis (reflectance vs. wavelength) data was used to calculate the band-gap of each material with the combined Kubelka-Munk and Tauc equation [111].

$$[\boldsymbol{F(r)} * \boldsymbol{hv}]^2 = [\frac{\boldsymbol{k}}{\boldsymbol{s}} * \boldsymbol{hv}]^2 = [\frac{\boldsymbol{(1-R)^2}}{\boldsymbol{2R}} * \boldsymbol{hv}]^2 \quad \boldsymbol{Where\ hv} = \frac{\boldsymbol{1240}}{\boldsymbol{\lambda}} \qquad \textbf{(3)}$$

Where F is Kubelka-Munk Function, % R is reflectance and hV is photon energy.

As shown in Table 3 and Figure 9, a large change in bandgap energy decreases to Cu-doped Cs_2SnCl_6 is doped (3.47 eV) from pure Cs_2SnCl_6 (4.19 eV).

Table 3 DRS result of un-doped and Cu doped Cs_2SnCl_6 PAL

Material	Bandgap (eV)
Pure PAL	4.19
0.10 Cu-PAL	3.87
0.15 Cu-PAL	3.76
0.20 Cu-PAL	3.47

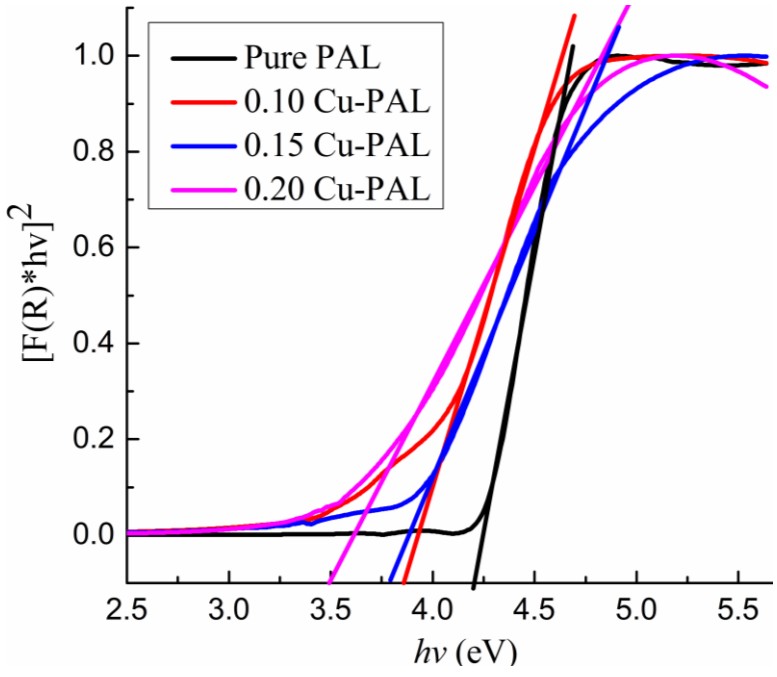

Figure 9 DRS result of Un-doped and Cu-doped Cs_2SnCl_6

The doping of both Cu and Co doesn't show a significant change in the crystal structure of ZnO due to the similarity in ionic radius and electronegativity between Zn, Co, and Cu. But the small shifting in band-gap was confirmed due to an electron exchange between band electrons of Zn lattice and the localized d-electrons of the transition-metal ion substituting the Zn with Co and Cu [111]. A pure ZnO bandgap of 3.24 eV was reduced to 3.06 eV for the Co-doped ZnO and 3.19 eV for Cu doped ZnO, which is shown in Table 4 and Figure 10.

Table 4 DRS result of undoped, Co-doped, Cu-doped ZnO

Material	Band Gap (eV)
Pure ZnO	3.24
Co-Z1	3.16
Co-Z2	3.06
Co-Z3	3.08
Co-Z5	3.12
Cu-Z1	3.23
Cu-Z2	3.19
Cu-Z3	3.22
Cu-Z5	3.21

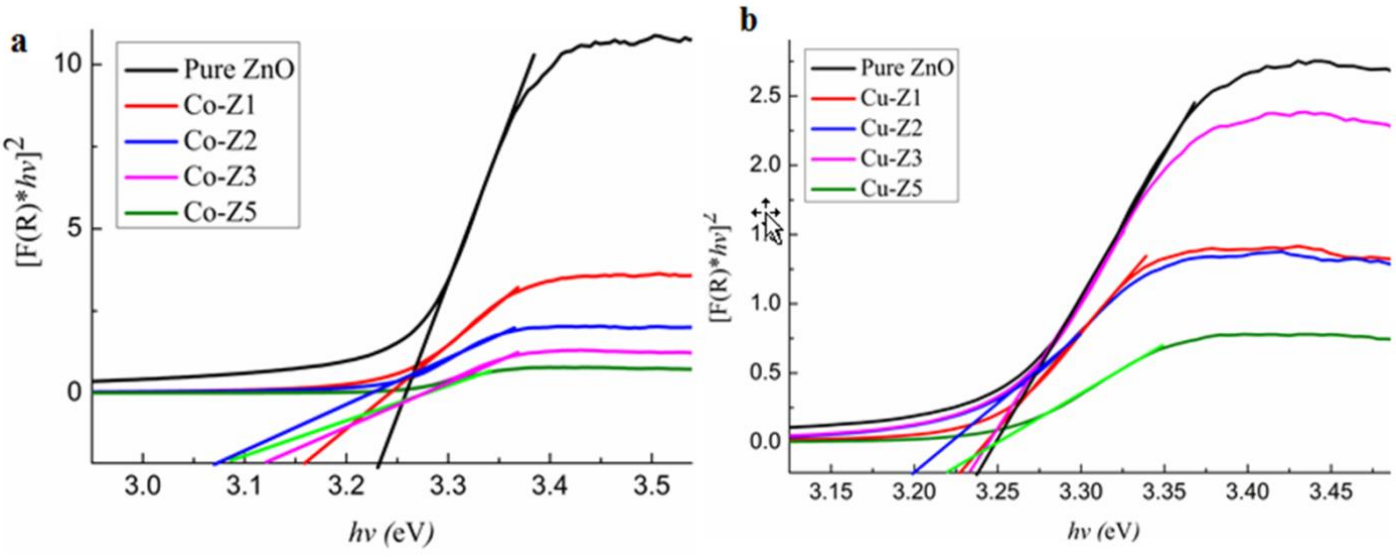

Figure 10 DRS result of (a) Co-doped and (b) Cu-doped ZnO

4.5. Photo-luminesce Spectroscopy (PL)

The PL spectroscopy analysis for un-doped and Cu-doped Cs_2SnCl_6 PAL was measured at the same excitation wavelength of 270 nm (Figure 11a), which shows the decreasing band-gap of wide Cs_2SnCl_6 dopant with dopant concentration. An additional peak observed at 397.5 nm (3.11ev), as shown in Figure 11b due to Cu doped in Cs_2SnCl_6 [13]. The other emission peak observed at 498 nm was observed, which is corresponds to a state of PAL in the $CsSnCl_3$ phase. The PL spectroscopy analysis shows a broadening and shifts with increasing dopant concentration as shown in Figure below [112]. The PL spectroscopy shows a shift to the higher wavelength region. For the 1st dopant where x=0.10 $Cs_2Sn_{1-x}Cu_xCl_6$ the shift was not significant. However, with a dopant where x=0.15 and 0.20 the shifts show a minor differencefor the same excitation wavelength. But the difference shows with the change of 5p electron configuration of Sn to exchange with Cu $3d^9\ 4s^2$ electron configuration as a dopant concentration increases.

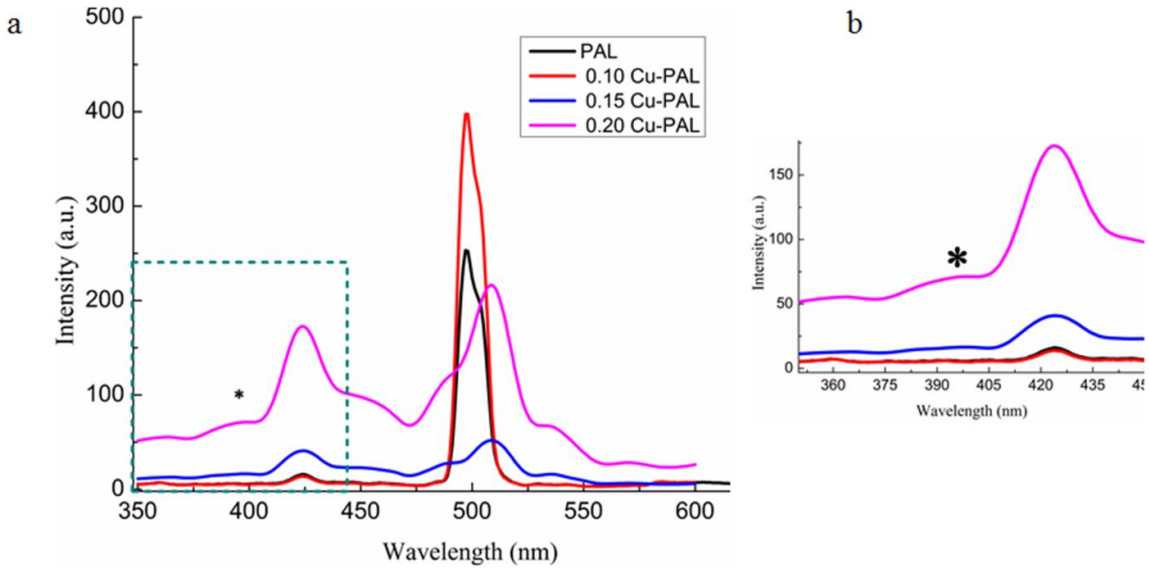

Figure 11 PL spectroscopy analysis of (a) undoped and Cu-doped Cs_2SnCl_6 (b)Magnified of undoped and Cu-doped Cs_2SnCl_6 at the new peak formation

And also a PL spectroscopy analysis was measured at an excitation wavelength of 325 nm for both un-doped and doped (Co and Cu) ZnO. The observation peak for Co-doped ZnO shows a decrease in intensity from increasing Co dopant concentration. ZnO observation peak is confirmed at 403 nm (UV-emission), 418 nm (Violet emission), 442 nm (Blue emission), and 494 nm (Blue emission). For Cu-doped ZnO the absorption peak appears at 404nm (UV-emission), 425 nm (Violet emission), 453 nm (Blue emission), 495 nm (Blue emission), and a green emission is formed at 529 nm. Even if the excitation wavelength doesn't change with

the dopant concentration, a doped ZnO ETL shows a shift in a blue emission peak was observed [113]. This shifting gives a clear confirmation of a bandgap decreases for doping of ZnO in DRS result [114]. The increase of a wide absorption peak observed in PL spectroscopy for all dopants in PAL and ETL forms the increase in recombination rate as shown in Figure 12 [115].

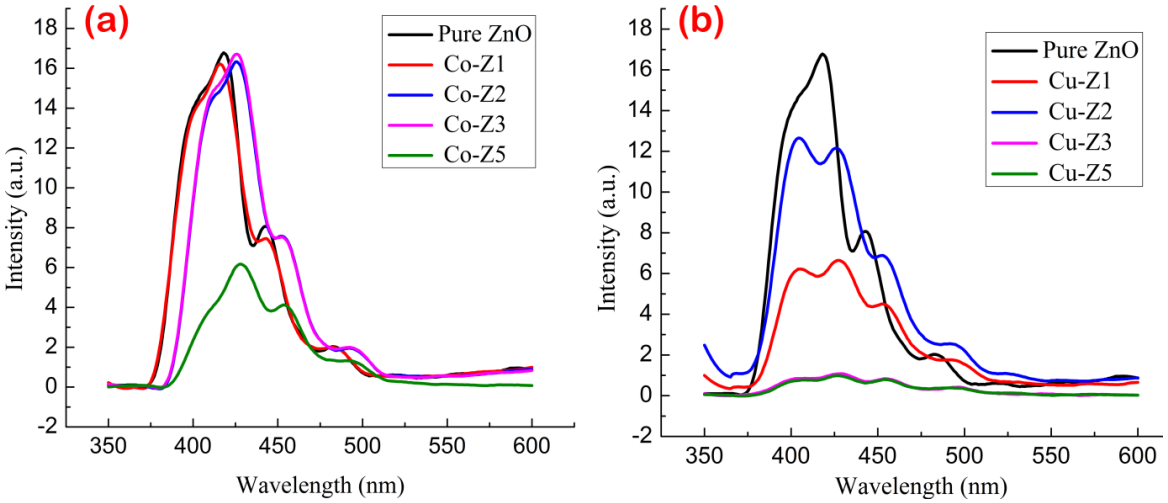

Figure 12 PL spectroscopy analysis of (a) Co-doped ZnO and (b) Cu-doped ZnO

4.6. Device Fabrication and I-V characterization

The general structure of a device mainly contains a configurational layer of perovskite absorption layer (PAL), an Electron Transport Layer, and a counter electrode. The device didn't include a Hole Transport Layer (HTL) due to a higher cost requirement and instability issue of HTL. A device of perovskite solar cell absorption layer of $Cs_2Sn_{1-x}Cu_xCl_6$ where x=0.20 is used for PSC device fabrication. For a selection of ETL, $Zn_{1-y}M_yO$ where M= Cu and Co and y= 0.01, 0.02, and 0.03 was selected for every M dopant of ZnO. The general device geometry and fabrication method were discussed on experimental procedure and it is shown in Figures 13 and 14 respectively. The *J-V* curve of all devices was first measured in a dark. After that, the solar simulator was calibrated to a one sun simulation of a solar cell at a radiant for J-V characterization.

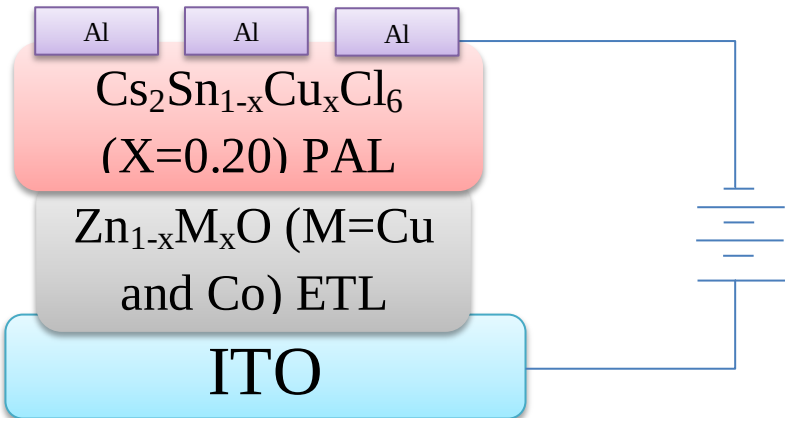

Figure 13 Device geometry of PSC device formed

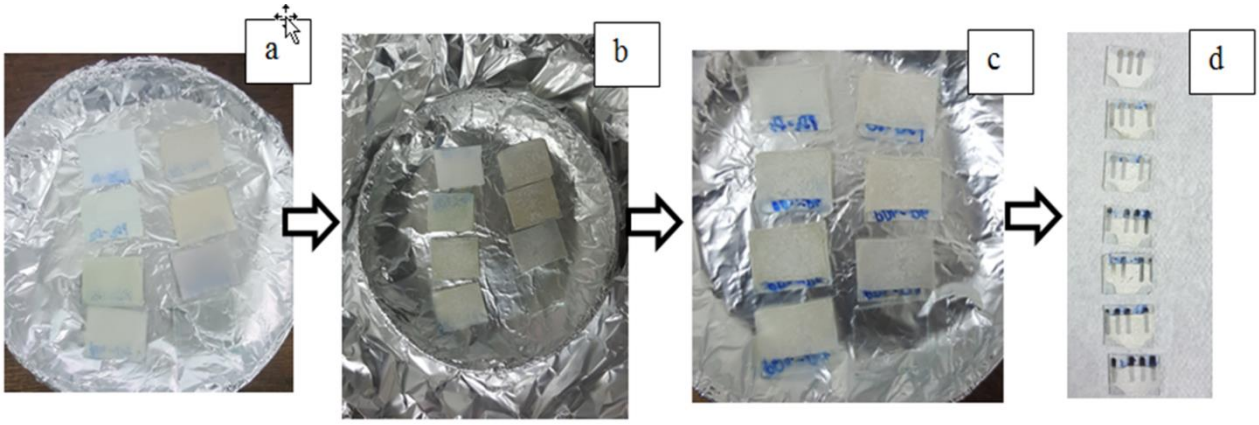

Figure 14 (a) $Zn_{1-y}M_yO$ (M=Cu and CO, y=0.01, 0.02 and 0.03) ETL spin coated on ITO, (b) $Cs_2Sn_{1-x}Cu_xCl_6$ (x=0.20) PAL spin coated on ETL, (c) bilayer cell after annaling, (d) Almunium electrode coated

The I-V curve of the selected PAL was used for device fabrication. And $Zn_{1-y}M_yO$ where (M= Co and Cu and y=0.00, 0.01, 0.02, and 0.03) ETL was used for the fabrication of a device. This was also necessary due to the undefined band structure of an A_2BX_6 structure perovskite material due to the PSC device depends on the band energy formed between the inter-junctional layer of the device. The Conduction Band Minima (CBM) and Valance Band Maxima (CBM) of $Cs_2Sn_{1-x}Cu_xCl_6$ were undefined as the new emerging A_2BX_6 PAL is still under investigation.

The I-V measurement of the device in the dark shows a current flow, which is relatively lower (microampere per cm^2) due to a wide bandgap structure of the PAL used for the device fabrication decreases the conductivity of the general device. As Cs_2SnCl_6 wide-bandgap nature of the material makes the device low conductive additional property of high recombination formed in the ETL and PAL interface. Even if, the enhancing with Co and Cu dope ZnO ETL for high electron carrier transport and performance of a PSC device shows some difference.

A difference between the Co-doped and Cu doped ZnO ETL was shown due to the higher recombination of Cu doped ZnO than Co-doped ZnO as shown in the PL spectroscopy result. The Co-doped ZnO ETL used PSC device had a relatively higher current flow than a Cu-doped ZnO ETL device fabricated with a similar voltage applied. But the difference is not significant, which mainly depends on the energy band and recombination formed by dopants of Co and Cu.

As the concentration of Cobalt doping increases the conductivity (decrease the resistivity) due to Co doping enhance the electron configuration, increases charge carrier, and allow the spontaneous polarization of unpolarized electron state of ZnO (due to the magnetic property of Co doping) [116-118]. As studies state, a Cu doping enhances the electro-optical property with the formation of impurity level near the conduction band minima or valance band maxima, which allows the conduction band minima (CBM) to moves downwards and the valance band maxima (VBM) to move upward. In addition to that the energy band structure of this PAL ($Cs_2Sn_{1-x}Cu_xCl_6$ where X=0.20) material is not defined. Whereas the Co doping shows a relatively lower moving of CBM downward [108].

Due to the difference in the conduction band minima position of Co and Cu doping ZnO ETL, an electron excited from the PAL can be affected. If the conduction band minima get further away from the conduction band of PAL, it forms an energy barrier where electrons to be transferred. The current density value of the device decreases as the CBM of the ETL is further moves downward due to a small number of electrons that can jump from the PAL to ETL to be collected. As shown in figure 15 (b), the Cu-doping ZnO ETL decreases in current density value compared to Co-doped in the J-V curve.

Even if the Co in ZnO ETL increases the current density further increasing the dopant concentration value decreases the current density (conductivity decreases) due to the recombination as an electron trap in the divalent Co^{2+} ion as shown in figure 15 (a) [119].

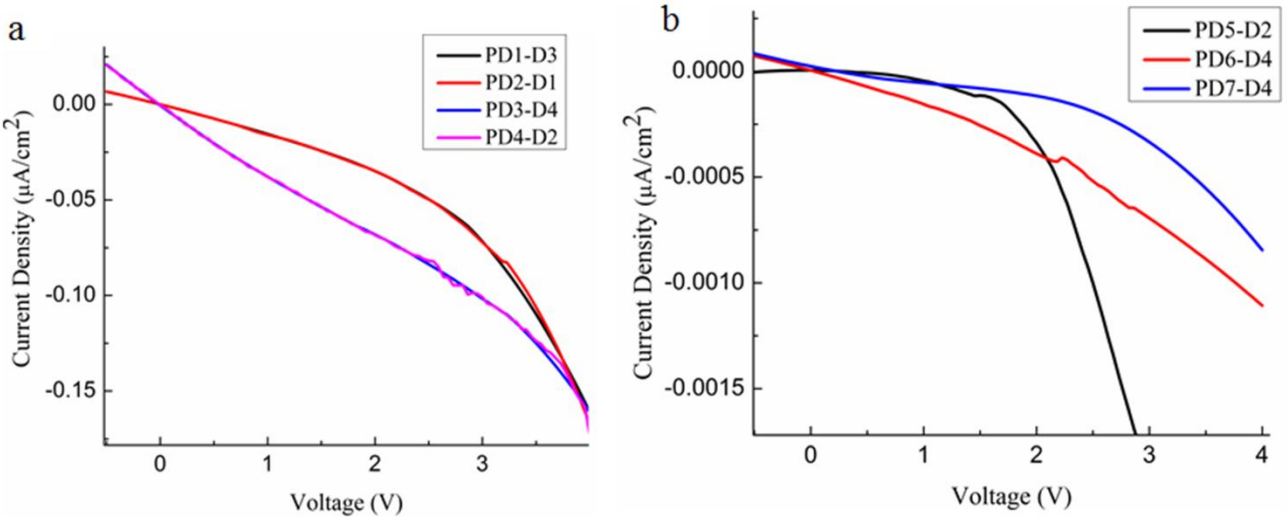

Figure 15 Dark I-V curve of (a) $Zn_{1-y}Co_yO$ (y=0.00, 0.01, 0.02 and 0.03), (b) $Zn_{1-y}Cu_yO$ (y=0.01, 0.02, 0.03)

An illumination of I-V analysis was also undertaken at 1-Sun radiant to analyze the performance of the PSC device fabricated as shown in Appendix 3. The result shows a very small (negligible) current density as shown in appendix 4, where a negative value is formed due to the low conductivity of PAL forms a high resistivity voltmeter. Where increasing in reistance can form a voltage drop. The increase in resistivity will form a reverse current flow as shown in Figure 16. The widewide bandgap nature makes the absorbance of the PAL in the UV wavelength range. which decreases the current density value due to the illumination of electron-hole pair generation. The wideband nature of this PAL also creates recombination of the generating electrons with a standard 1-Sun radiant light in a visible range, which limits the formation of the electron-hole pairs to be collected. And also affects the excitation of electrons to be conducted, which requires high energy to form an excitation.

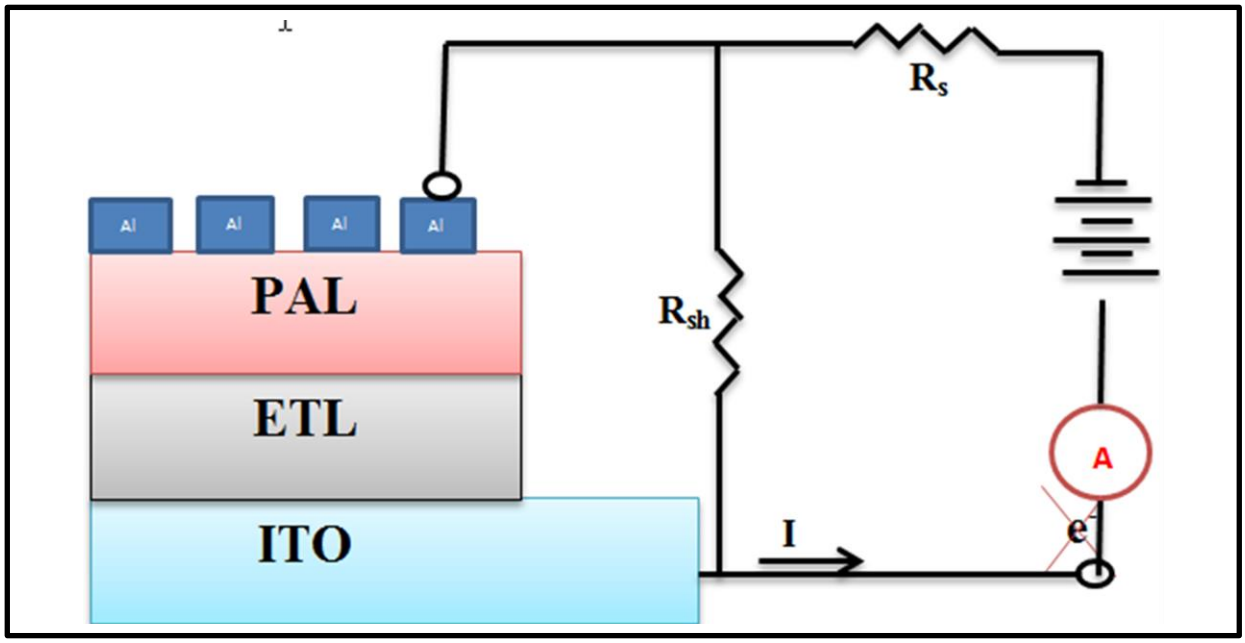

Figure 16 Circuit diagram for Illumnation of solar light on PD3 and PD4

5. Conclusions and Recommendations

5.1. Conclusions

A $Cs_2Sn_{1-x}Cu_xCl_6$ (where x= 0.10, 0.15, 0.20 and 0.25) perovskite absorption layer (PAL) and $Zn_{1-y}M_yO$ (where M= Co and Cu, y= 0.01, 0.02, 0.03 and 0.05) is synthesized with a co-precipitation method at 350^{o}c for PAL, and ZnO ETL at 400^{o}c for Co-doped ZnO and also 500^{o}c for Cu-ZnO ETL. The synthesized powders are characterized by XRD, SEM, DTG, UV-Vis Spectroscopy, and PL Spectroscopy. The XRD result of PAL shows a Cubic crystal, in which six cubics FCC forms an orthogonal morphology confirmed by SEM analysis. The orthogonal structure is formed as the synthesizing of the PAL is occurred at a particular HCl concentration of 3mol/L. The XRD result of ETL shows a Wurtzite Hexagonal structure. The thermal analysis of PAL shows a promising result of A_2BX_6 structure thermal stability at 550^{o}c. Also, the thermal property of un-doped and doped ZnO ETL is analyzed using DTG. Co-doped ZnO (Co-Z3) shows better stability with 3% Co-doped ZnO due to the less mass loss with only 2.763% than a Cu doped ZnO 3% doped (5.421%). The optical property of PAL and ETL is analyzed by DRS and PL Spectroscopy method. The different orientation analyzed method of DRS and PL Spectroscopy gives a different result of the bandgap. DRS result shows a decrease in bandgap as the dopant concentration increases. A 0.20Cu doped Cs_2SnCl_6 PAL shows the decrease of the bandgap to be 3.47 eV from 4.19 eV of pure Cs_2SnCl_6 PAL. This result will also be confirmed by PL spectroscopy analysis, in which an additional Peak is formed at 397.52nm (3.11 eV). The doped ETL also shows a decrease in bandgap as the concentration of heavy metal dopants increases. After a certain amount of decrease, the bandgap shows an increased value. The Co-doped ZnO at 0.02Co doped ZnO (Co-Z2) shows a decrease value of 3.06 eV relatively to 3.24 eV of Pure ZnO and Cu-Z2 of Cu doped ZnO of 3.19 eV. This analysis of synthesized PAL and ETL shows doping affects the optical property higher than the thermal property. So the performance of the PSC device can be enhanced without reducing thermal stability. Even if doping shows an enhancing optical property but it shows a limitation for device fabrication. The J-V curve of device analysis shows that as the dopant concentration increases the current density (current) decreases due to the increase in a junction energy barrier, which limits the transfer of electrons from a PAL to ETL. On other hand, the negative value under illumination can occur as a result of low conductivity and mismatch of the energy band. So a band energy property of Cs_2SnCl_6 to ETL must be further analyzed. Doping of ETL can decrease the bandgap (moves the CBM downward) which forms a large energy barrier between the two (PAL and ETL) junction.

5.2. Recommendation and Further works

To meet the commercial demand of solar cell devices, which achieving both stable and efficient solar cell devices using a proper selection of material is required. A stable material like Cs_2SnCl_6 become attracts many scholars, due to a stable for of Sn^{4+} oxidation state and in this work, it has proven a higher thermal stable property even using Cu dopants for better optical performance. One drawback of this material is the wide bandgap optical structure makes it less efficient. So selecting and finding a better dopant to reduce the bandgap, which can form a high absorption on photon energy in the visible range is required. And also the study of degradation in moisture and illumination are still yet to study. Another best way of forming a better efficient PSC device is selecting a proper ETL material. A compatible junctional layer (lower energy barrier) between the PAL and ETL can enhance the performance of the solar cell.

A study of the band structure of both PAL and ETL is necessary to find the defined device configuration. Especially for a PAL material used in this thesis ($Cs_2Sn_{1-x}Cu_xCl_6$ where x=0.20), the band structure of the material is undefined. So current and XPS analysis is being undertaken to analyze the band structure and oxidation state of the material. After analyzing those results a Quenching Effect is analyzed and calculation will be performed using PL-spectroscopy to find the best configuration of PAL and ETL for the device fabrication. Additionally, the doping of both PAL and ETL must be analyzed using dopant analyzer instruments like Transmission Electron Microscope. Besides, the grain size of the undoped and doped ZnO ETL must be analyzed using Scanning Electron Microscope (SEM), which can analysis in nanoscale.

Reference

1. Lebelhuber, C. and H. Steinmüller, How and to which extent can the gas sector contribute to a climate-neutral European energy system? A qualitative approach. Energy, Sustainability and Society, 2019. 9(1): p. 23.
2. Parida, B., S. Iniyan, and R. Goic, A review of solar photovoltaic technologies. Renewable and sustainable energy reviews, 2011. 15(3): p. 1625-1636.
3. Chang, X., *et al*., Carbon-Based $CsPbBr_3$ Perovskite Solar Cells: All-Ambient Processes and High Thermal Stability. ACS Appl Mater Interfaces, 2016. 8(49): p. 33649-33655.
4. Kojima, A., *et al*., Organometal halide perovskites as visible-light sensitizers for photovoltaic cells. Journal of the American Chemical Society, 2009. 131(17): p. 6050-6051.
5. Yao, Y., W.-L. Hsu, and M. Dagenais, High-Efficiency Perovskite Solar Cell Based on Sequential Doping of PTAA. IEEE Journal of Photovoltaics, 2019. 9(4): p. 1025-1030.
6. Kandjani, S.A., S. Mirershadi, and A. Nikniaz, Inorganic–organic perovskite solar cells. Solar Cells-New Approaches and Reviews, 2015: p. 450.
7. Yin, W.-J., *et al*., Halide perovskite materials for solar cells: a theoretical review. Journal of Materials Chemistry A, 2015. 3(17): p. 8926-8942.
8. Saparov, B., *et al*., Thin-film deposition and characterization of a Sn-deficient perovskite derivative Cs_2SnI_6. Chemistry of Materials, 2016. 28(7): p. 2315-2322.
9. Zhang, H., *et al*., Morphologically Controlled Synthesis of Cs_2SnCl_6 Perovskite Crystals and Their Photoluminescence Activity. Crystals, 2019. 9(5): p. 258.
10. Kaltzoglou, A., *et al*., Optical-vibrational properties of the Cs_2SnX_6 (X= Cl, Br, I) defect perovskites and hole-transport efficiency in dye-sensitized solar cells. The Journal of Physical Chemistry C, 2016. 120(22): p. 11777-11785.
11. Lee, B., *et al*., Air-stable molecular semiconducting iodosalts for solar cell applications: Cs2SnI6 as a hole conductor. Journal of the American Chemical Society, 2014. 136(43): p. 15379-15385.
12. Li, J., *et al*., Antimony doped Cs_2SnCl_6 with bright and stable emission. Frontiers of Optoelectronics, 2019. 12(4): p. 352-364.
13. Tan, Z., *et al*., Highly efficient blue-emitting Bi-doped Cs_2SnCl_6 perovskite variant: photoluminescence induced by impurity doping. Advanced Functional Materials, 2018. 28(29): p. 1801131.

14. Noh, M.F.M., *et al.*, The architecture of the electron transport layer for a perovskite solar cell. Journal of Materials Chemistry C, 2018. 6(4): p. 682-712.
15. Harrison, S.E., Conductivity and Hall effect of ZnO at low temperatures. Physical Review, 1954. 93(1): p. 52.
16. Krishnan, U., *et al.*, Factors affecting the stability of perovskite solar cells: a comprehensive review. Journal of Photonics for Energy, 2019. 9(2): p. 021001.
17. Chen, J., *et al.*, Recent progress in stabilizing hybrid perovskites for solar cell applications. Journal of Power Sources, 2017. 355: p. 98-133.
18. Sans, J., *et al.*, Chemical effects on the optical band-gap of heavily doped ZnO: M III (M= Al, Ga, In): an investigation by means of photoelectron spectroscopy, optical measurements under pressure, and band structure calculations. Physical Review B, 2009. 79(19): p. 195105.
19. Zhao, X., *et al.*, Aluminum-doped zinc oxide as highly stable electron collection layer for perovskite solar cells. ACS applied materials & interfaces, 2016. 8(12): p. 7826-7833.
20. Song, J., *et al.*, Magnesium-doped Zinc Oxide as Electron Selective Contact Layers for Efficient Perovskite Solar Cells. ChemSusChem, 2016. 9(18): p. 2640-2647.
21. Mahmood, K. and A. Khalid, Single-step electrospray deposited nitrogen-doped ZnO nanosheets yield hysteresis-free perovskite solar cells. Materials Letters, 2018. 224: p. 78-81.
22. Park, S., R. Kang, and S. Cho, Effect of an Al-doped ZnO electron transport layer on the efficiency of inverted bulk heterojunction solar cells. Current Applied Physics, 2020. 20(1): p. 172-177.
23. Wang, Z., *et al.*, Urea-Doped ZnO Films as the Electron Transport Layer for High Efficiency Inverted Polymer Solar Cells. Front Chem, 2018. 6: p. 398.
24. Wang, L., *et al.*, Indium Zinc Oxide Electron Transport Layer for High-Performance Planar Perovskite Solar Cells. The Journal of Physical Chemistry C, 2018. 122(50): p. 28491-28496.
25. Su, T., *et al.*, Band Engineering via Sn-doping of Zinc Oxide Electron Transport Materials for Perovskite Solar Cells. ChemistrySelect, 2018. 3(2): p. 363-367.
26. Zhou, Z. and S. Pang, Highly efficient inverted hole-transport-layer-free perovskite solar cells. Journal of Materials Chemistry A, 2020. 8(2): p. 503-512.

27. Xu, T., *et al*., Strategic improvement of the long-term stability of perovskite materials and perovskite solar cells. Physical Chemistry Chemical Physics, 2016. 18(39): p. 27026-27050.
28. Bisquert, J. and E.J. Juarez-Perez, The causes of degradation of perovskite solar cells. 2019, ACS Publications.
29. Berhe, T.A., *et al*., Organometal halide perovskite solar cells: degradation and stability. Energy & Environmental Science, 2016. 9(2): p. 323-356.
30. Lu, Y.-B., *et al*., Light enhanced moisture degradation of perovskite solar cell material CH 3 NH 3 PbI 3. Journal of Materials Chemistry A, 2019. 7(48): p. 27469-27474.
31. Chen, C.J., Physics of solar energy. 2011: John Wiley & Sons.
32. Green, M.A., *et al*., Solar cell efficiency tables (version 37). Progress in photovoltaics: research and applications, 2010. 1(19): p. 84-92.
33. Czochralski, J., Ein neues verfahren zur messung der kristallisationsgeschwindigkeit der metalle. Zeitschrift für physikalische Chemie, 1918. 92(1): p. 219-221.
34. Green, M.A., *et al*., Solar cell efficiency tables (version 52). Progress in Photovoltaics: Research and Applications, 2018. 26(7): p. 427-436.
35. Ryu, S., *et al*., Fabrication of metal-oxide-free $CH_3NH_3PbI_3$ perovskite solar cells processed at low temperature. Journal of Materials Chemistry A, 2015. 3(7): p. 3271-3275.
36. Kim, H.-S., *et al*., Lead iodide perovskite sensitized all-solid-state submicron thin film mesoscopic solar cell with efficiency exceeding 9%. Scientific reports, 2012. 2(1): p. 1-7.
37. Filip, M.R. and F. Giustino, The geometric blueprint of perovskites. Proceedings of the National Academy of Sciences, 2018. 115(21): p. 5397-5402.
38. Snaith, H.J., Present status and future prospects of perovskite photovoltaics. Nature materials, 2018. 17(5): p. 372-376.
39. Jeon, N.J., *et al*., Solvent engineering for high-performance inorganic-organic hybrid perovskite solar cells. Nature materials, 2014. 13(9): p. 897-903.
40. Yuan, D.-X., *et al*., Inverted planar NH 2 CH [double bond, length as m-dash] NH_2 PbI_3 perovskite solar cells with 13.56% efficiency via low-temperature processing. Physical Chemistry Chemical Physics, 2015. 17(30): p. 19745-19750.
41. Gonzalez-Pedro, V., *et al*., General working principles of CH3NH3PbX3 perovskite solar cells. Nano letters, 2014. 14(2): p. 888-893.

42. Cai, Y., *et al*., Computational study of halide perovskite-derived A_2BX_6 inorganic compounds: chemical trends in electronic structure and structural stability. Chemistry of Materials, 2017. 29(18): p. 7740-7749.
43. Zhou, H., *et al*., Interface engineering of highly efficient perovskite solar cells. Science, 2014. 345(6196): p. 542-546.
44. Marinova, N., S. Valero, and J.L. Delgado, Organic and perovskite solar cells: Working principles, materials and interfaces. Journal of colloid and interface science, 2017. 488: p. 373-389.
45. Wu, W.-Q., *et al*., Molecular doping enabled scalable blading of efficient hole-transport-layer-free perovskite solar cells. Nature communications, 2018. 9(1): p. 1-8.
46. Asad, J., *et al*., Perovskite solar cells free of hole transport layer. Journal of Sol-Gel Science and Technology, 2019. 90(3): p. 443-449.
47. Wu, C., *et al*., The Dawn of Lead-Free Perovskite Solar Cell: Highly Stable Double Perovskite $Cs_2AgBiBr_6$ Film. Advanced Science, 2018. 5(3): p. 1700759.
48. Shao, D., *et al*., A high performance UV–visible dual-band photodetector based on an inorganic Cs_2SnI_6 perovskite/ZnO heterojunction structure. Journal of Materials Chemistry C, 2020. 8(5): p. 1819-1825.
49. Kojima, A., *et al*., Organometal halide perovskites as visible-light sensitizers for photovoltaic cells. 2009. 131(17): p. 6050-6051.
50. Jeon, N.J., *et al*., Compositional engineering of perovskite materials for high-performance solar cells. Nature, 2015. 517(7535): p. 476.
51. Jeon, N.J., *et al*., A fluorene-terminated hole-transporting material for highly efficient and stable perovskite solar cells. Nature Energy, 2018. 3(8): p. 682.
52. Pellet, N., *et al*., Mixed-organic-cation Perovskite photovoltaics for enhanced solar-light harvesting. Angewandte Chemie International Edition, 2014. 53(12): p. 3151-3157.
53. Brivio, F., C. Caetano, and A. Walsh, Thermodynamic origin of photoinstability in the $CH_3NH_3Pb(I1–x\ Br\ x)_3$ hybrid halide perovskite alloy. The journal of physical chemistry letters, 2016. 7(6): p. 1083-1087.
54. Wu, Z., *et al*., Stabilizing the $CsSnCl_3$ Perovskite Lattice by B-Site Substitution for Enhanced Light Emission. Chemistry of Materials, 2019. 31(14): p. 4999-5004.
55. Rajagopal, A., K. Yao, and A.K. Jen, Toward Perovskite Solar Cell Commercialization: A Perspective and Research Roadmap Based on Interfacial Engineering. Adv Mater, 2018. 30(32): p. e1800455.

56. Mesquita, I., L. Andrade, and A. Mendes, Temperature Impact on Perovskite Solar Cells Under Operation. ChemSusChem, 2019. 12(10): p. 2186-2194.
57. Lee, J.-W., *et al.*, Formamidinium and Cesium Hybridization for Photo- and Moisture-Stable Perovskite Solar Cell. Advanced Energy Materials, 2015. 5(20): p. 1501310.
58. Conings, B., *et al.*, Intrinsic Thermal Instability of Methylammonium Lead Trihalide Perovskite. Advanced Energy Materials, 2015. 5(15): p. 1500477.
59. Ouedraogo, N.A.N., *et al.*, Stability of all-inorganic perovskite solar cells. Nano Energy, 2020. 67: p. 104249.
60. Zhang, Q., *et al.*, Perovskite solar cells: must lead be replaced - and can it be done? Science and technology of advanced materials, 2018. 19(1): p. 425-442.
61. Kour, R., *et al.*, Potential substitutes for replacement of lead in perovskite solar cells: a review. Global Challenges, 2019. 3(11): p. 1900050.
62. Kulbak, M., D. Cahen, and G. Hodes, How Important Is the Organic Part of Lead Halide Perovskite Photovoltaic Cells? Efficient $CsPbBr_3$ Cells. J Phys Chem Lett, 2015. 6(13): p. 2452-6.
63. Kulbak, M., D. Cahen, and G. Hodes, How important is the organic part of lead halide perovskite photovoltaic cells? Efficient $CsPbBr_3$ cells. The journal of physical chemistry letters, 2015. 6(13): p. 2452-2456.
64. Sutton, R.J., *et al.*, Bandgap-tunable cesium lead halide perovskites with high thermal stability for efficient solar cells. Advanced Energy Materials, 2016. 6(8): p. 1502458.
65. Noel, N.K., *et al.*, Lead-free organic–inorganic tin halide perovskites for photovoltaic applications. Energy & Environmental Science, 2014. 7(9): p. 3061-3068.
66. Xing, G., *et al.*, Solution-Processed Tin-Based Perovskite for Near-Infrared Lasing. Advanced Materials, 2016. 28(37): p. 8191-8196.
67. Qiu, X., *et al.*, Lead-free mesoscopic Cs_2SnI_6 perovskite solar cells using different nanostructured ZnO nanorods as electron transport layers. physica status solidi (RRL)–Rapid Research Letters, 2016. 10(8): p. 587-591.
68. Sabba, D., *et al.*, Impact of anionic Br–substitution on open circuit voltage in lead free perovskite ($CsSnI_{3-x}Br_x$) solar cells. The Journal of Physical Chemistry C, 2015. 119(4): p. 1763-1767.
69. Chen, Z., *et al.*, Schottky solar cells based on $CsSnI_3$ thin-films. Applied Physics Letters, 2012. 101(9): p. 093901.

70. Yan, L., *et al.*, Interface Engineering for All-Inorganic $CsPbI_2Br$ Perovskite Solar Cells with Efficiency over 14. Adv Mater, 2018: p. e1802509.
71. Xiao, Z., *et al.*, Searching for promising new perovskite-based photovoltaic absorbers: the importance of electronic dimensionality. Materials Horizons, 2017. 4(2): p. 206-216.
72. Qiu, X., *et al.*, From unstable $CsSnI_3$ to air-stable Cs_2SnI_6: A lead-free perovskite solar cell light absorber with bandgap of 1.48 eV and high absorption coefficient. Solar Energy Materials and Solar Cells, 2017. 159: p. 227-234.
73. Scott, S.M., *et al.*, The thermal stability and consolidation of perovskite variant Cs_2SnCl_6 using spark plasma sintering. Journal of the American Ceramic Society, 2018. 101(5): p. 2060-2065.
74. Zhu, W., *et al.*, Tunable optical properties and stability of lead free all inorganic perovskites ($Cs_2SnIxCl_{6-x}$). Journal of Materials Chemistry A, 2018. 6(6): p. 2577-2584.
75. Jinghui, L., *et al.*, Antimony doped Cs_2SnCl_6 with bright and stable. Frontiers of Optoelectronics, 2019. 12(4): p. 352–364.
76. Wang, A., *et al.*, Controlled synthesis of lead-free and stable perovskite derivative Cs_2SnI_6 nanocrystals via a facile hot-injection process. Chemistry of Materials, 2016. 28(22): p. 8132-8140.
77. Zhou, Y., *et al.*, Ultrabroad photoluminescence and electroluminescence at new wavelengths from doped organometal halide perovskites. The journal of physical chemistry letters, 2016. 7(14): p. 2735-2741.
78. Özgür, Ü., *et al.*, A comprehensive review of ZnO materials and devices. Journal of applied physics, 2005. 98(4): p. 11.
79. Yuan, Z., Low-temperature synthesis of ZnO nanoparticles for inverted polymer solar cell application. Journal of Materials Science: Materials in Electronics, 2014. 25(3): p. 1289-1292.
80. Chen, L.-C. and Z.-L. Tseng, ZnO-Based Electron Transporting Layer for Perovskite Solar Cells. 2017.
81. Zhao, Y.-h., *et al.*, Comprehensive Study of Sol–Gel versus Hydrolysis–Condensation Methods To Prepare ZnO Films: Electron Transport Layers in Perovskite Solar Cells. ACS Applied Materials & Interfaces, 2017. 9(31): p. 26234-26241.
82. Chi, D., *et al.*, Ultra-thin ZnO film as an electron transport layer for realizing the high efficiency of organic solar cells. RSC advances, 2017. 7(24): p. 14694-14700.

83. Liang, L., *et al*., Magnetron sputtered zinc oxide nanorods as thickness-insensitive cathode interlayer for perovskite planar-heterojunction solar cells. ACS applied materials & interfaces, 2014. 6(23): p. 20585-20589.
84. Liu, D. and T. Kelly, Perovskite solar cells with a planar heterojunction structure prepared using room-temperature solution processing techniques–supporting information, Nat. Photonics 8 (2013) 133–138. 2013.
85. Jurablu, S., M. Farahmandjou, and T. Firoozabadi, Sol-gel synthesis of zinc oxide (ZnO) nanoparticles: a study of structural and optical properties. Journal of Sciences, Islamic Republic of Iran, 2015. 26(3): p. 281-285.
86. Jayappa, M.D., *et al*., Green synthesis of zinc oxide nanoparticles from the leaf, stem and in vitro grown callus of Mussaenda frondosa L.: characterization and their applications. Applied Nanoscience, 2020: p. 1-18.
87. Haque, M.J., *et al*., Synthesis of ZnO nanoparticles by two different methods & comparison of their structural, antibacterial, photocatalytic and optical properties. Nano Express, 2020. 1(1): p. 010007.
88. Rouchdi, M., *et al*., Synthesis and characteristics of Mg doped ZnO thin films: Experimental and ab-initio study. Results in physics, 2017. 7: p. 620-627.
89. Gionco, C., *et al*., Synthesis, characterization, and photocatalytic tests of N-doped zinc oxide: a new interesting photocatalyst. Journal of Nanomaterials, 2016. 2016.
90. Ji, X., *et al*., Fabrication of high-performance F and Al co-doped ZnO transparent conductive films for use in perovskite solar cells. Solar Energy Materials and Solar Cells, 2019. 190: p. 6-11.
91. Morvillo, P., *et al*., Solution-processed indium doped zinc oxide as electron transport layer for inverted polymer solar cells. 2016.
92. Wu, J., M. Wang, and K.-L. Choy, The study of novel doped ZnO for perovskite solar cells Institution of Materials Discovery. 2017.
93. Xin, Y., *et al*., A review of the perovskite solar cells. Acta Physica Sinica, 2015. 64(3).
94. Cahen, D., *et al*., Nature of photovoltaic action in dye-sensitized solar cells. The Journal of Physical Chemistry B, 2000. 104(9): p. 2053-2059.
95. Chen, L.-C., *et al*., Effect of Different CH3NH3PbI3 Morphologies on Photovoltaic Properties of Perovskite Solar Cells. Nanoscale Research Letters, 2018. 13.

96. Bahtiar, A., *et al.* Structural properties of perovskite films on zinc oxide nanoparticles-reduced graphene oxide (ZnO-NPs/rGO) prepared by electrophoretic deposition technique. in AIP Conference Proceedings. 2018. AIP Publishing.
97. Wang, Z., *et al.*, Urea-Doped ZnO Films as the Electron Transport Layer for High Efficiency Inverted Polymer Solar Cells. Frontiers in Chemistry, 2018. 6: p. 398.
98. Mahmud, M.A., *et al.*, Solution-processed lithium-doped ZnO electron transport layer for efficient triple cation (Rb, MA, FA) perovskite solar cells. ACS applied materials & interfaces, 2017. 9(39): p. 33841-33854.
99. Chouhan, A.S., N.P. Jasti, and S. Avasthi. Ozone-Treated Aluminum Doped Zinc Oxide for ETL-Free Stable Perovskite Solar Cells. in 2018 IEEE 7th World Conference on Photovoltaic Energy Conversion (WCPEC)(A Joint Conference of 45th IEEE PVSC, 28th PVSEC & 34th EU PVSEC). 2018. IEEE.
100. Lee, M.M., *et al.*, Efficient hybrid solar cells based on meso-superstructured organometal halide perovskites. Science, 2012. 338(6107): p. 643-647.
101. Burschka, J., *et al.*, Sequential deposition as a route to high-performance perovskite-sensitized solar cells. Nature, 2013. 499(7458): p. 316.
102. Shukla, P., *et al.*, Investigation on structural, morphological and optical properties of Co-doped ZnO thin films. Physica B: Condensed Matter, 2018. 550: p. 303-310.
103. Zhang, Y., L. Mi, and Z. Zheng, Study on the structure and optical property of $Zn_{1-x}Cu_xO$ sol–gel thin films on quartz substrate. Physica B: Condensed Matter, 2012. 407(12): p. 2254-2257.
104. Ullah, S., *et al.*, Fabrication and characterization of lead-free Cs_2SnI_6 perovskite films for photovoltaic applications. International Journal of Energy Research, 2020.
105. Vaiano, V., G. Iervolino, and L. Rizzo, Cu-doped ZnO as an efficient photocatalyst for the oxidation of arsenite to arsenate under visible light. Applied Catalysis B: Environmental, 2018. 238: p. 471-479.
106. Speaks, D., Effect of concentration, aging, and annealing on sol gel ZnO and Al-doped ZnO thin films. International Journal of Mechanical and Materials Engineering, 2020. 15(1): p. 1-14.
107. Oku, T., Crystal structures of $CH_3NH_3PbI_3$ and related perovskite compounds used for solar cells. Solar Cells-New Approaches and Reviews, 2015. 1.
108. Ma, Z., *et al.*, Cu-doped ZnO electronic structure and optical properties studied by first-principles calculations and experiments. Materials, 2019. 12(1): p. 196.

109. Niu, G., *et al*., Enhancement of thermal stability for perovskite solar cells through cesium doping. RSC advances, 2017. 7(28): p. 17473-17479.
110. Sajjad, M., *et al.*, Structural and optical properties of pure and copper doped zinc oxide nanoparticles. Results in Physics, 2018. 9: p. 1301-1309.
111. Makuła, P., M. Pacia, and W. Macyk, How to correctly determine the band gap energy of modified semiconductor photocatalysts based on UV–Vis spectra. 2018, ACS Publications.
112. Lin, T.-W., C. Su, and C.C. Lin, Phase transition and energy transfer of lead-free Cs_2SnCl_6 perovskite nanocrystals by controlling the precursors and doping manganese ions. Journal of Information Display, 2019. 20(4): p. 209-216.
113. Mahroug, A., *et al.*, Structural, morphological and optical properties of undoped and Co-doped ZnO thin films prepared by sol–gel process. Journal of Materials Science: Materials in Electronics, 2014. 25(11): p. 4967-4974.
114. He, J.H., *et al*., Large-scale Ni-doped ZnO nanowire arrays and electrical and optical properties. Journal of the American Chemical Society, 2005. 127(47): p. 16376-16377.
115. Doan, M.T., X.V. Ho, and T. Nguyen, Influence of doping Co to characterization of ZnO nanostructures. Advances in Natural Sciences: Nanoscience and Nanotechnology, 2014. 5(2): p. 025011.
116. Khan, M.S., L.-j. Shi, and B. Zou, First principles calculations of optoelectronic and magnetic properties of Co-doped and (Co, Al) co-doped ZnO. Journal of Applied Physics, 2020. 127(6): p. 065707.
117. Kaphle, A., *et al*., Doping Efficiency in Cobalt-Doped ZnO Nanostructured Materials. Journal of Nanomaterials, 2019. 2019.
118. Wu, Z.H., H.Q. Xie, and Y.B. Zhai, *Preparation and Thermoelectric Properties of Co-Doped ZnO Synthesized by Sol-Gel.* J Nanosci Nanotechnol, 2015. 15(4): p. 3147-50.
119. Godavarti, U., V. Mote, and M. Dasari, *Role of cobalt doping on the electrical conductivity of ZnO nanoparticles.* Journal of Asian Ceramic Societies, 2017. 5(4): p. 391-396.

Appendices

Appendix I

Crystallographic Informations of Cs_2SnCl_6

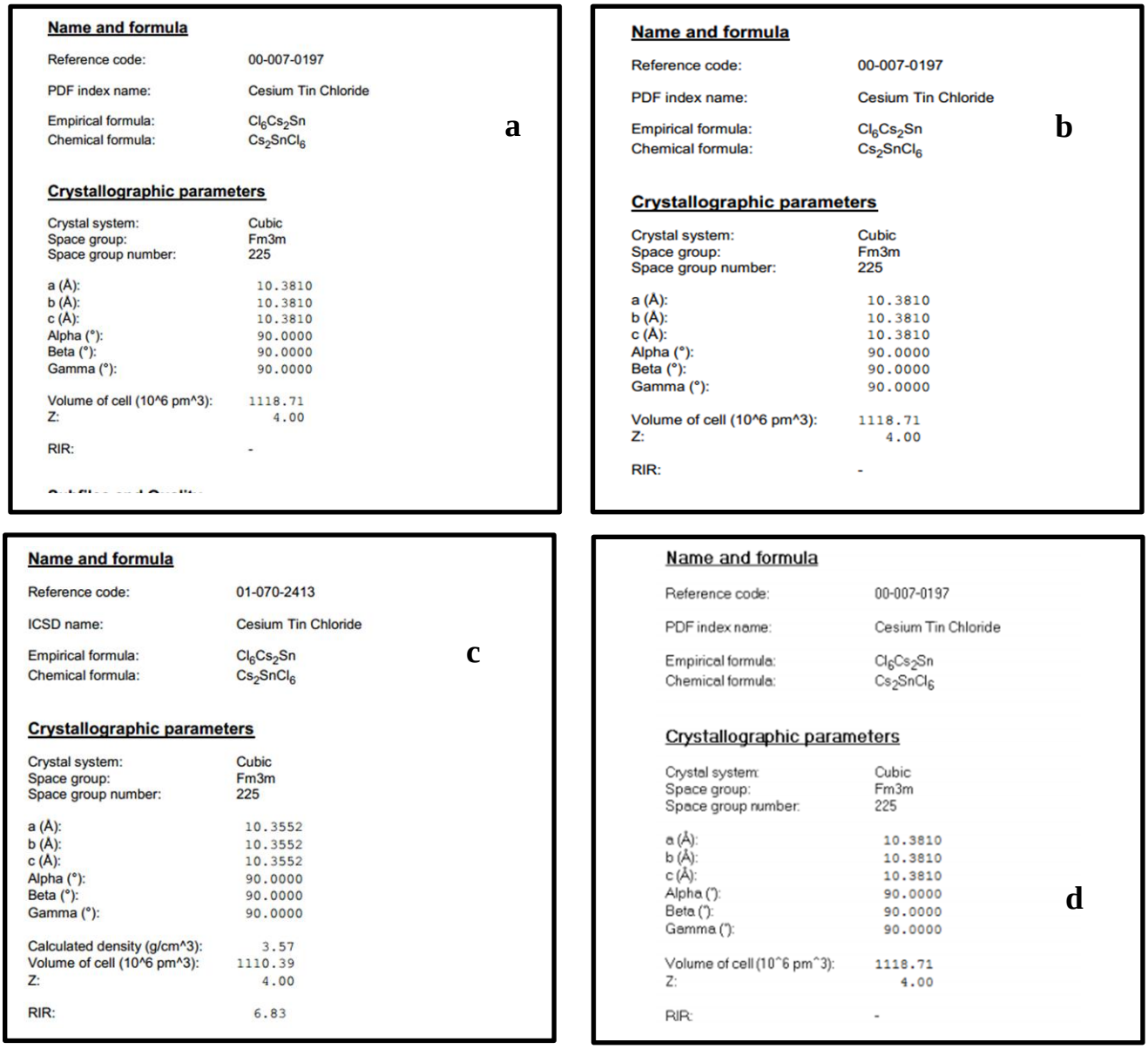

Name and formula

Reference code: 00-007-0197
PDF index name: Cesium Tin Chloride
Empirical formula: Cl_6Cs_2Sn
Chemical formula: Cs_2SnCl_6

Crystallographic parameters

Crystal system: Cubic
Space group: Fm3m
Space group number: 225

a (Å): 10.3810
b (Å): 10.3810
c (Å): 10.3810
Alpha (°): 90.0000
Beta (°): 90.0000
Gamma (°): 90.0000

Volume of cell (10^6 pm^3): 1118.71
Z: 4.00

RIR: -

a

Name and formula

Reference code: 00-007-0197
PDF index name: Cesium Tin Chloride
Empirical formula: Cl_6Cs_2Sn
Chemical formula: Cs_2SnCl_6

Crystallographic parameters

Crystal system: Cubic
Space group: Fm3m
Space group number: 225

a (Å): 10.3810
b (Å): 10.3810
c (Å): 10.3810
Alpha (°): 90.0000
Beta (°): 90.0000
Gamma (°): 90.0000

Volume of cell (10^6 pm^3): 1118.71
Z: 4.00

RIR: -

b

Name and formula

Reference code: 01-070-2413
ICSD name: Cesium Tin Chloride
Empirical formula: Cl_6Cs_2Sn
Chemical formula: Cs_2SnCl_6

Crystallographic parameters

Crystal system: Cubic
Space group: Fm3m
Space group number: 225

a (Å): 10.3552
b (Å): 10.3552
c (Å): 10.3552
Alpha (°): 90.0000
Beta (°): 90.0000
Gamma (°): 90.0000

Calculated density (g/cm^3): 3.57
Volume of cell (10^6 pm^3): 1110.39
Z: 4.00

RIR: 6.83

c

Name and formula

Reference code: 00-007-0197
PDF index name: Cesium Tin Chloride
Empirical formula: Cl_6Cs_2Sn
Chemical formula: Cs_2SnCl_6

Crystallographic parameters

Crystal system: Cubic
Space group: Fm3m
Space group number: 225

a (Å): 10.3810
b (Å): 10.3810
c (Å): 10.3810
Alpha (°): 90.0000
Beta (°): 90.0000
Gamma (°): 90.0000

Volume of cell (10^6 pm^3): 1118.71
Z: 4.00

RIR: -

d

Figure 17 Appendix X-pert analysis of XRD of (a) Pure PAL (b) 0.10Cu-PAL (0.15Cu=PAL) (C) 0.15Cu-PAL and (d) 0.20Cu-PAL

Appendix II

Crystallographic Information of ZnO

a

Name and formula

Reference code:	01-079-2205
ICSD name:	Zinc Oxide
Empirical formula:	OZn
Chemical formula:	ZnO

Crystallographic parameters

Crystal system:	Hexagonal
Space group:	P63mc
Space group number:	186
a (Å):	3.2501
b (Å):	3.2501
c (Å):	5.2071
Alpha (°):	90.0000
Beta (°):	90.0000
Gamma (°):	120.0000
Calculated density (g/cm^3):	5.67
Volume of cell (10^6 pm^3):	47.63
Z:	2.00
RIR:	5.41

b

Name and formula

Reference code:	01-079-0205
ICSD name:	Zinc Oxide
Empirical formula:	OZn
Chemical formula:	ZnO

Crystallographic parameters

Crystal system:	Hexagonal
Space group:	P63mc
Space group number:	186
a (Å):	3.2417
b (Å):	3.2417
c (Å):	5.1876
Alpha (°):	90.0000
Beta (°):	90.0000
Gamma (°):	120.0000
Calculated density (g/cm^3):	5.72
Volume of cell (10^6 pm^3):	47.21
Z:	2.00
RIR:	5.65

c

Name and formula

Reference code:	01-076-0704
ICSD name:	Zinc Oxide
Empirical formula:	OZn
Chemical formula:	ZnO

Crystallographic parameters

Crystal system:	Hexagonal
Space group:	P63mc
Space group number:	186
a (Å):	3.2530
b (Å):	3.2530
c (Å):	5.2130
Alpha (°):	90.0000
Beta (°):	90.0000
Gamma (°):	120.0000
Calculated density (g/cm^3):	5.66
Volume of cell (10^6 pm^3):	47.77
Z:	2.00
RIR:	5.42

d

Name and formula

Reference code:	01-076-0704
ICSD name:	Zinc Oxide
Empirical formula:	OZn
Chemical formula:	ZnO

Crystallographic parameters

Crystal system:	Hexagonal
Space group:	P63mc
Space group number:	186
a (Å):	3.2530
b (Å):	3.2530
c (Å):	5.2130
Alpha (°):	90.0000
Beta (°):	90.0000
Gamma (°):	120.0000
Calculated density (g/cm^3):	5.66
Volume of cell (10^6 pm^3):	47.77
Z:	2.00

e

Name and formula

Reference code:	01-076-0704
ICSD name:	Zinc Oxide
Empirical formula:	OZn
Chemical formula:	ZnO

Crystallographic parameters

Crystal system:	Hexagonal
Space group:	P63mc
Space group number:	186
a (Å):	3.2530
b (Å):	3.2530
c (Å):	5.2130
Alpha (°):	90.0000
Beta (°):	90.0000
Gamma (°):	120.0000
Calculated density (g/cm^3):	5.66
Volume of cell (10^6 pm^3):	47.77
Z:	2.00
RIR:	5.42

f

Name and formula

Reference code:	01-076-0704
ICSD name:	Zinc Oxide
Empirical formula:	OZn
Chemical formula:	ZnO

Crystallographic parameters

Crystal system:	Hexagonal
Space group:	P63mc
Space group number:	186
a (Å):	3.2530
b (Å):	3.2530
c (Å):	5.2130
Alpha (°):	90.0000
Beta (°):	90.0000
Gamma (°):	120.0000
Calculated density (g/cm^3):	5.66
Volume of cell (10^6 pm^3):	47.77
Z:	2.00

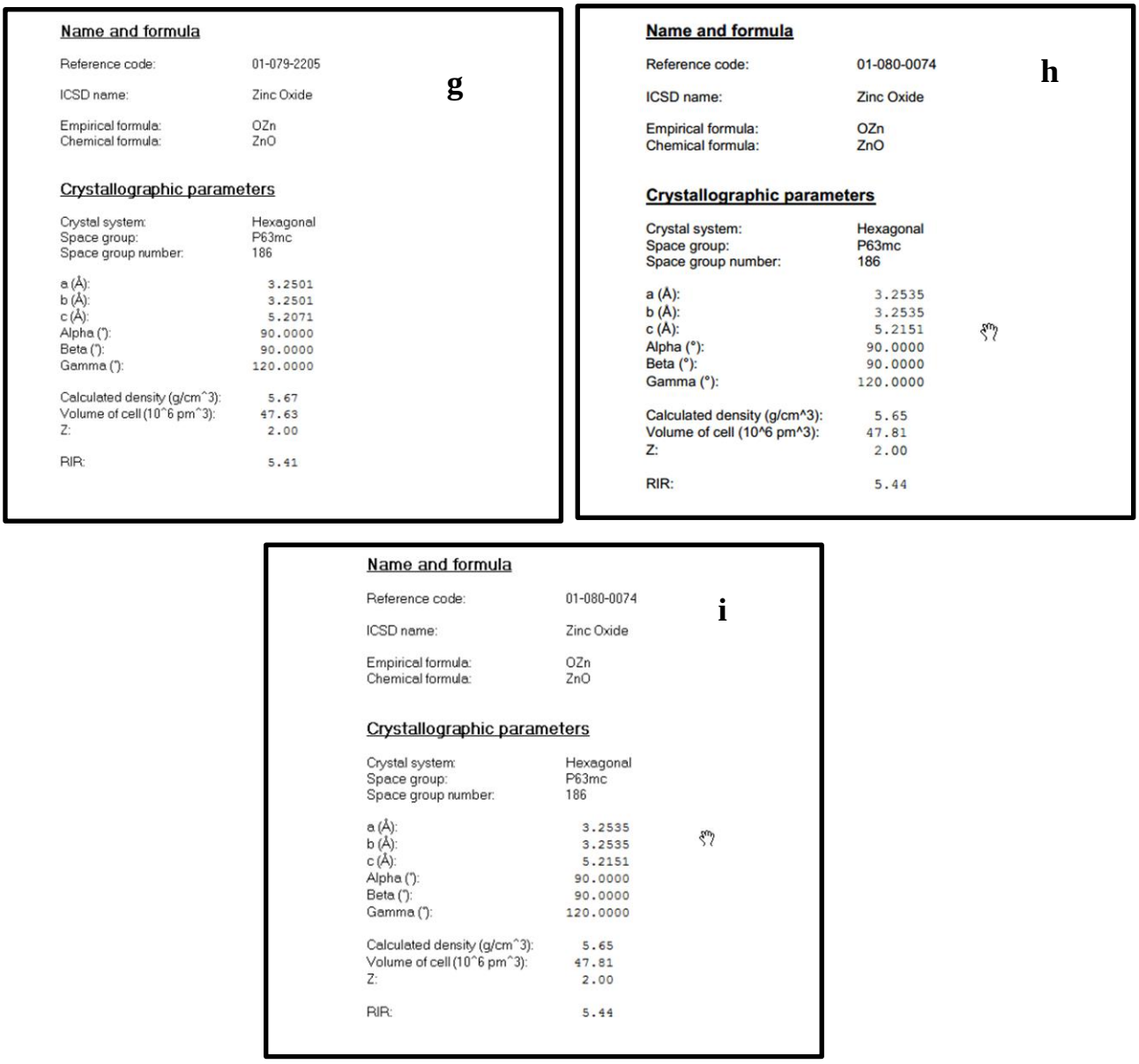

Figure 18 ZnO ETL X-pert High score XRD analysis (a) Pure ZnO, (b) Co=Z1, (c) Co=Z2, (d) Co=Z3, (e) Co=Z5, (f) Cu=Z1, (g) Cu=Z2, (h) Cu=Z3, (i) Cu=Z5

Appendix III

Experimental set-up of device performance evaluation

Figure 19 Device performance measuring setup

Appendix IV

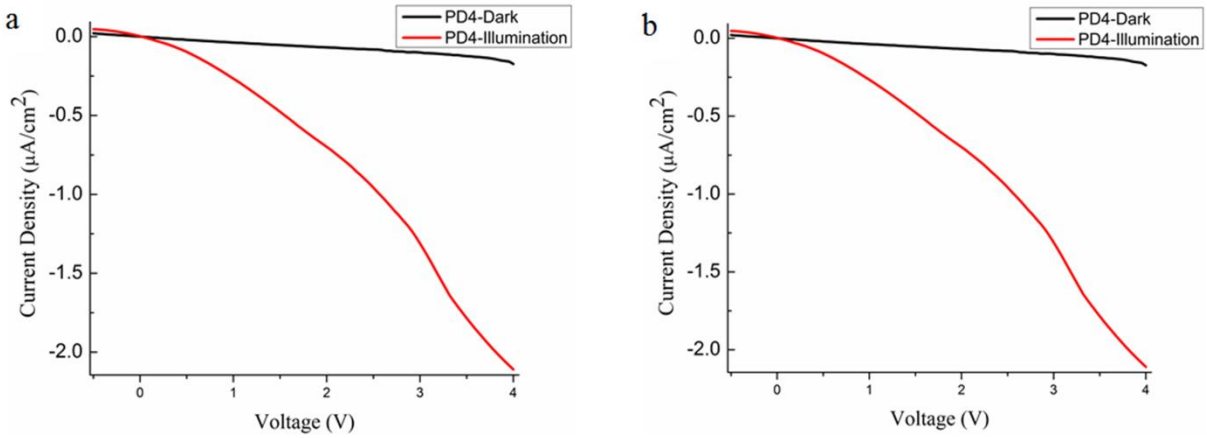

Figure 20 Current Density Vs Voltage of dark and Illumination of (a) for PD3 and (b) for PD4